arXiv:1702.02701v1 [math.NA] 9 Feb 2017

A POSTERIORI ERROR ESTIMATION AND ADAPTIVE ALGORITHM FOR THE ATOMISTIC/CONTINUUM COUPLING IN 2D

H. WANG, M. LIAO, P. LIN, AND L. ZHANG

Abstract. Atomistic/continuum coupling methods aim to achieve optimal balance between accuracy and efficiency. Adaptivity is the key for the efficient implementation of such methods. In this paper, we carry out a rigorous a posterior error analysis which includes the residual estimate, the stability constant estimate and the error bound, for a consistent atomistic/continuum coupling method in 2D. Adaptive mesh refinement algorithm can be designed correspondingly and the convergence rate with respect to degrees of freedom is optimal compare with a priori error estimates.

1. Introduction

Atomistic/continuum (a/c) coupling methods are a class of computational multiscale methods that aim to combine the accuracy of the atomistic model and the efficiency of the continuum model for crystalline solids with defects [25, 42, 12]. To be precise, the atomistic model can be applied in a small neighborhood of the localized defects such as vacancies, dislocations, and cracks, while the continuum model (e.g., Cauchy-Born rule) can be employed away from the defect cores where elastic deformation occurs. The construction and analysis of different a/c coupling methods have attracted considerable attention in the research community in recent years [15, 29, 18, 17]. We refer the readers to [22, 19] for a review of such methods.

The goal of the mathematical analysis is to find the optimal relation of accuracy vs. degrees of freedom. The a priori analysis has been given for several typical a/c coupling methods, for example the QNL method (quasi-nonlocal quasicontinuum method) [23, 34], the BQCE method (blended energy-based quasi-continuum method) [14], the BQCF method (blended force-based quasi-continuum method) [17, 14], the GRAC method (geometric reconstruction based atomistic/continuum coupling) [36] and the BGFC method (atomistic/continuum blending with ghost force correction) [38]. In contrast, only few research articles are concerned with the a posteriori error control of the these methods. Prudhomme et al. [39] uses the goal-oriented approach to provide a posteriori error control for a three dimensional nanoindentation problem with the quantity of interest being the force acting on the

Date: February 10, 2017.

2000 *Mathematics Subject Classification.* 65N12, 65N15, 70C20, 82D25.

Key words and phrases. atomistic models, coarse graining, atomistic-to-continuum coupling, quasicontinuum method, a posteriori error estimate.

HW was partially supported by NSFC grant 11501389, 11471214 and Sichuan University Starting Up Research Funding No. 2082204194117. PL and ML were partially supported by NSFC grant 91430106 and Fundamental Research Funds for Central Universities Nos. 06108038 and FRF-BR-13-023. PL and HW were partially supported by EMS RSF grant. LZ was partially supported by NSFC grant 11471214, 11571314 and the One Thousand Plan of China for young scientists.

indenter. The error estimator, whose effectiveness is validated only numerically, is given as a modification of a rigorous derived residual functional. Arndt and Luskin [1, 2] use the same approach to analytically derive the a posteriori error estimates for a one dimensional Frenkel-Kontorova model. The goal oriented a posteriori error estimators are used to optimize the choice of the atomistic region as well as the finite element mesh in the continuum region. All of these work employ the original energy-based quasicontinuum method as the underlying model which is later shown to be inconsistent [6, 23, 21]. Recently, Kochmann et al. [45] proposed an adaptivity strategy for the so-call "fully-nonlocal quasi-continuum" method which apply a discrete model in the entire computational domain without coupling of different models. Such method is in a slightly different spirit from the problem we consider in the present work.

The a posteriori error bounds in the energy norms are first derived in [32, 26] through a similar approach as the present work for two different types of coupling schemes which are (later characterized in [16]) the QCP method and the QNL method. However, the QCP method analyzed in [32] only contains finite element discretization without the coupling of different models while the extension to higher dimensions of the scheme in [26] is not clear. A recent advance in this direction [35] is the a posteriori error analysis of a consistent energy-based coupling method developed in [40, 41], where the a posteriori error estimators in the energy norm and in energy itself were proposed.

Despite all those developments, the rigorous mathematical justification of a posteriori error estimate beyond 1D is still missing. In this paper, we present a rigorous a posteriori error estimate for a consistent energy-based a/c method in two dimension which is of physical significance, and has not been considered so far to the best knowledge of the authors. We use the residual-based approach [46] to establish the estimate in negative Sobolev norms following [35]. Two features distinguish our problem from the classic residual-based estimate for finite element approximation of the elliptic equations. The first one is the existence of the modeling error which is in origin different from the applications of quadrature rules. The second one is that the mesh may not be further refined when it almost coincides with the reference lattice but a model adaptation should be imposed. The 2D results rely on the analysis and implementation of divergence free field, which characterize the essential difference of 2D compared with 1D results in [26, 35], where the analysis can be carried out by explicit calculations.

Similar to the a priori analysis of GRAC in [36], we constrain ourselves to the case of nearest-neighbor interactions. Although the analysis can be extended to finite range interactions and to other a/c coupling methods, we decide not to include these so that the main ideas and steps are clearly presented without the distraction from the unnecessary complexity of the presentation.

The paper is organized as follows. In § 2 we set up the atomistic, continuum and coupling models for point defects. In § 3.1 we derive the residual for the coupling scheme. In § 3.2 we obtain the stability bound for the coupling method, and then, in § 3.3 we present rigorous a posteriori error estimates. We present the numerical algorithms and results in § 4 and we give the conclusion and the outlook of our work in § 5. Some auxiliary results are given in § 6.

2. Formulation

We will first give a brief review of a model for crystal defects in an infinite lattice in the spirit of [9] in § 2.1 and the Cauchy-Born continuum model in § 2.2. We then present a generic form of a/c coupling schemes in § 2.3, the consistent scheme GRAC will be introduced specifically in § 2.4.

2.1. **Atomistic model.**

2.1.1. *Atomistic lattice and defects.* Given $d \in \{2, 3\}$, $\mathsf{A} \in \mathbb{R}^{d\times d}$ non-singular, $\Lambda^{\mathrm{hom}} := \mathsf{A}\mathbb{Z}^d$ is the *homogeneous reference lattice* which represents a perfect *single lattice crystal* formed by identical atoms and possessing no defects. $\Lambda \subset \mathbb{R}^d$ is the *reference lattice* with some local *defects*. The mismatch between Λ and Λ^{hom} represents possible defects Λ^{def}, which are contained in some localized *defect cores* D^{def} such that the atoms in $\Lambda\backslash D^{\mathrm{def}}$ do not interact with defects Λ^{def} (see § 2.1.2 and § 2.1.3 regarding interaction neighbourhood). For example, $\Lambda^{\mathrm{def}} = \{x\}$ for a crystal with a single point defect at x, and one can choose a proper radius $R^{\mathrm{def}} > 0$ such that $D^{\mathrm{def}} = B_{x,R^{\mathrm{def}}}$, where $B_{x,R} := \{z \in \mathbb{R}^d \,|\, |z - x| \leqslant R\}$. For different types of point defects, we have

- $\Lambda \subset \Lambda^{\mathrm{hom}}$ for a vacancy at $x \in \Lambda^{\mathrm{hom}}$;
- $\Lambda \supset \Lambda^{\mathrm{hom}}$ for an interstitial at $x \in \Lambda$ but $x \notin \Lambda^{\mathrm{hom}}$;
- $\Lambda = \Lambda^{\mathrm{hom}}$ for an impurity at $x \in \Lambda^{\mathrm{hom}}$, the difference of the impurity atom with other atoms can be characterized by the inhomogeneity of interaction potentials (§ 2.1.3)

This characterization of localized defects can be straightforwardly generalized to multiple point defects and micro-cracks, for example, see the setup of the model problem in § 4.2. Straight screw dislocations can be enforced through the appropriate choice of boundary conditions [9].

2.1.2. *Lattice function and lattice function space.* Given $d \in \{2, 3\}$, $m \in \{1, 2, 3\}$, denote the set of vector-valued *lattice functions* by

$$\mathscr{U} := \{v : \Lambda \to \mathbb{R}^m\}.$$

A *deformed configuration* is a *lattice function* $y \in \mathscr{U}$. Let x be the identity map, the *displacement* $u \in \mathscr{U}$ is defined by $u(\ell) = y(\ell) - x(\ell) = y(\ell) - \ell$ for any $\ell \in \Lambda$.

For each $\ell \in \Lambda$, prescribe an *interaction neighbourhood* $\mathcal{N}_\ell := \{\ell' \in \Lambda \,|\, 0 < |\ell' - \ell| \leqslant r_{\mathrm{cut}}\}$ with some cut-off radius r_{cut}. The *interaction range* $\mathcal{R}_\ell := \{\ell' - \ell \,|\, \ell' \in \mathcal{N}_\ell\}$ is defined as the union of lattice vectors defined by the finite difference of lattice points in $\mathcal{N}_\ell$ and ℓ.

To measure the error for lattice functions we need to introduce function norms and function spaces on the lattice. Define the "finite difference stencil" $Dv(\ell) := \{D_\rho v(\ell)\}_{\rho\in\mathcal{R}_\ell} := \{v(\ell + \rho) - v(\ell)\}_{\rho\in\mathcal{R}_\ell}$. Higher-order finite differences, e.g., $D_\rho D_\varsigma v$ and $D^2 v$ can be defined in a canonical way. A *lattice function norm* can hence be defined using those notations. For $v \in \mathscr{U}$, let the lattice energy-norm (a discrete H^1-semi-norm) be

$$\|Dv\|_{\ell^2} := \left(\sum_{\ell\in\Lambda}\sum_{\rho\in\mathcal{R}_\ell} \frac{|D_\rho v(\ell)|^2}{|\rho|^2}\right)^{1/2}. \tag{2.1}$$

The associated *lattice function space* is defined by

$$\dot{\mathscr{U}}^{1,2} := \big\{u : \Lambda \to \mathbb{R}^m \,\big|\, \|Du\|_{\ell^2} < +\infty\big\}.$$

We choose

$$\mathcal{B} := \{(\ell, \ell+\rho) : \ell \in \Lambda, \rho \in \mathcal{R}_\ell\} \tag{2.2}$$

to be the collection of all the nearest neighbour bonds in the reference lattice, and for $b = (\ell, \ell+\rho) \in \mathcal{B}$, denote $\rho_b = \rho$. Then the energy norm can be reformulated as

$$\|Dv\|_{\ell^2} := \bigg(\sum_{b=(\ell,\ell+\rho)\in\mathcal{B}} \frac{|D_\rho v(\ell)|^2}{|\rho|^2}\bigg)^{1/2}. \tag{2.3}$$

The homogeneous lattice $\Lambda^{\rm hom} = \mathsf{A}\mathbb{Z}^d$ naturally induces a simplicial micro-triangulation $\mathcal{T}$. In 2D, $\mathcal{T}^{\rm a} = \{\mathsf{A}\xi + \hat{T}, \mathsf{A}\xi - \hat{T} | \xi \in \mathbb{Z}^2\}$, where $\hat{T} = \mathrm{conv}\{0, e_1, e_2\}$. Let $\bar{\zeta} \in W^{1,\infty}(\Lambda^{\rm hom}; \mathbb{R})$ be the P1 nodal basis function associated with the origin; namely, $\bar{\zeta}$ is piecewise linear with resepct to $\mathcal{T}^{\rm a}$, and $\bar{\zeta}(0) = 1$ and $\bar{\zeta}(\xi) = 0$ for $\xi \neq 0$ and $\xi \in \Lambda^{\rm hom}$. The nodal interpolant of $v \in \mathscr{U}$ can be written as

$$\bar{v}(x) := \sum_{\xi\in\mathbb{Z}^d} v(\xi)\bar{\zeta}(x-\xi).$$

We can introduce the discrete homogeneeous Sobolev spaces

$$\mathscr{U}^{1,2} := \{u \in \mathscr{U} | \nabla \bar{u} \in L^2\},$$

with semi-norm $\|\nabla \bar{u}\|_{L^2}$. It is know from [30] that $\dot{\mathscr{U}}^{1,2}$ and $\mathscr{U}^{1,2}$ are equivalent.

2.1.3. *Interaction potential.* For each $\ell \in \Lambda$, let $V_\ell(u)$ denote the *site energy* associated with the lattice site $\ell \in \Lambda$. In this paper, we consider the general multibody interaction potential of the *generic pair functional form* [44]. Namely, the potential is a function of the distances between atoms within interaction range and there is no angular dependence. Accordingly, we have the following equivalent forms of interaction potentials,

$$V_\ell(u) = \widehat{V}_\ell(\{D_\rho u(\ell)\}_{\rho\in\mathcal{R}_\ell}) = \widetilde{V}_\ell(\{|D_\rho u(\ell)|\}_{\rho\in\mathcal{R}_\ell}) \tag{2.4}$$

Remark 2.1. For convenience, with a slight abuse of notation, we will use $V_\ell(D_\rho u)$, $V_\ell(|D_\rho u|)$ instead of $\widehat{V}_\ell(\{D_\rho u(\ell)\}_{\rho\in\mathcal{R}_\ell})$, $\widetilde{V}_\ell(\{|D_\rho u(\ell)|\}_{\rho\in\mathcal{R}_\ell})$ when there is no confusion in the context. □

A great number of practical potentials are in the form (2.4), including the widely used Embedded Atom Model (EAM) [5] and Finnis-Sinclair model [11]. For example, assuming a finite interaction neighborhood $\mathcal{N}_\ell$ and an interaction range $\mathcal{R}_\ell$ for $\ell \in \Lambda$, EAM potential reads

$$\begin{aligned} V_\ell(u) &:= \sum_{\ell'\in\mathcal{N}_\ell} \phi(|u(\ell) - u(\ell')|) + F\Big(\textstyle\sum_{\ell'\in\mathcal{N}_\ell} \psi(|u(\ell) - u(\ell')|)\Big), \\ &= \sum_{\rho\in\mathcal{R}_\ell} \phi\big(|D_\rho u(\ell)|\big) + F\Big(\textstyle\sum_{\rho\in\mathcal{R}_\ell} \psi\big(|D_\rho u(\ell)|\big)\Big). \end{aligned} \tag{2.5}$$

for a pair potential ϕ, an electron density function ψ and an embedding function F. The potential V_ℓ is *homogeneous* outside the defect region $D^{\rm def}$, namely, $V_\ell = V$ and $\mathcal{R}_\ell = \mathcal{R}$ for $\ell \in \Lambda \backslash D^{\rm def}$. V and $\mathcal{R}$ have the following symmetry: $\mathcal{R} = -\mathcal{R}$, and $V(\{-g_{-\rho}\}_{\rho\in\mathcal{R}}) = V(g)$.

The energy of an infinite configuration is typically ill-defined. However, if we redefine the potential $V_\ell(u)$ as the difference $V_\ell(u) - V_\ell(0)$, which is equivalent to assuming $V_\ell(0) = 0$, the energy functional

$$\mathscr{E}^{\rm a}(u) = \sum_{\ell\in\Lambda} V_\ell(u) \tag{2.6}$$

is a meaningful object. By [9, Lemma 2.1], given some natural technical assumptions for the site potentials V_ℓ, $\mathscr{E}^{\rm a}(u)$ is well-defined for $u \in \mathscr{U}^{1,2}$, and if $V_\ell(u)$ is C^k in its variables, $\mathscr{E}^{\rm a}$ is k times Fréchet differentiable. In particular, we define M as the Lipschitz constant of $\delta^2\mathscr{E}^{\rm a}$.

Under the above conditions, the goal of the atomistic problem is to find a *strongly stable* equilibrium u, such that

$$u \in \arg\min \left\{ \mathscr{E}^{\rm a}(u) \,\middle|\, u \in \mathscr{U}^{1,2} \right\}. \tag{2.7}$$

We call u *strongly stable* if there exists $c_0 > 0$ such that

$$\langle \delta^2\mathscr{E}^{\rm a}(u)v, v\rangle \geqslant c_0 \|\nabla v\|_{L^2}^2, \quad \forall v \in \mathscr{U}^{1,2}.$$

.

It is proven in [9, Theorem 2.3] that, if the homogeneous lattice is stable, for a critical point $u \in \mathscr{U}^{1,2}$ of $\mathscr{E}^{\rm a}$, $D^j u$, $j = 0, 1, \ldots$ exhibit the following *generic decay*,

$$\left|D^j u(\ell)\right| \lesssim |\ell|^{1-d-j}, \quad \text{and} \quad \left|u(\ell) - u_\infty\right| \lesssim |\ell|^{-d+1}. \tag{2.8}$$

where $u_\infty := \lim_{|\ell|\to\infty} u(\ell)$.

2.2. **Continuum model.** Let V be the homogeneous site potential outside the defect core. To formulate atomistic to continuum coupling schemes we require a continuum model compatible with (2.6) defined through a strain energy density function $W : \mathbb{R}^{d\times d} \to \mathbb{R}$. A typical choice in the multi-scale context is the Cauchy–Born model [8, 33], the energy density W in the homogeneous crystal $\mathsf{F}\Lambda^{\rm hom} = \mathsf{F}\mathsf{A}\mathbb{Z}^d$ is defined by

$$W(\mathsf{F}) := \det \mathsf{A}^{-1} V(\mathsf{F}x).$$

2.3. **A/C coupling.** We begin by giving a generic formulation of an a/c coupling method and employ concepts and notation from various earlier works, such as [25, 42, 43, 20, 37], but adapt the formulation to the settings in this paper.

First, we choose a computational domain Ω_R: let $\Omega_R \subset \mathbb{R}^d$ be a simply connected, polygonal and closed set, such that $B_{0,R} \subset \Omega_R \subset B_{0,c_0R}$ for some $c_0 > 0$. We decompose $\Omega_R = \Omega_R^{\rm a} \bigcup \Omega_R^{\rm c}$, where the atomistic region $\Omega_R^{\rm a}$ is again simply connected and polygonal, and contains the defect core: $D^{\rm def} \subset \Omega_R^{\rm a}$. Let $R_{\rm a}$ be the radius of $\Omega_R^{\rm a}$. Take $\mathcal{T}_{h,R}^c$ as a regular simplicial partition (triangles for $d = 2$ or tetrahedra for $d = 3$) of the continuum region $\Omega_R^{\rm c}$.

Next, we decompose the set of atoms $\Lambda^{\rm a,i} := \Lambda \bigcap \Omega_R^{\rm a} = \Lambda^{\rm a} \bigcup \Lambda^{\rm i}$ into a core atomistic set $\Lambda^{\rm a}$ and an interface set $\Lambda^{\rm i}$ (typically a few "layers" of atoms surrounding $\Lambda^{\rm a}$) such that $\Lambda^{\rm i} \bigcap D^{\rm def} = \varnothing$. Let $\mathcal{T}_{h,R}^{\rm a}$ be the triangulation of $\Omega_R^{\rm a}$ induced by $\Lambda^{\rm a,i}$. $\mathcal{T}_{h,R} = \mathcal{T}_{h,R}^{\rm c} \bigcup \mathcal{T}_{h,R}^{\rm a}$ is the associated triangulation of Ω_R. Sometimes, it is also useful to define $\mathcal{T}_{h,R}^{\rm i} := \{T \in \mathcal{T}_{h,R} : \Lambda^{\rm i} \bigcap T \neq \varnothing\}$. Please see Figure 1 for an illustration of the computational mesh.

We may use $\mathcal{T}_h$ instead of $\mathcal{T}_{h,R}$ by dropping the subscript R if there is no confusion. Let $\mathcal{N}_h$ be the set of nodes in $\mathcal{T}_h$, and $\mathcal{F}_h$ be the set of edges in $\mathcal{T}_h$.

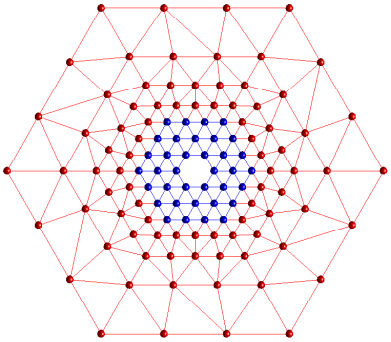

FIGURE 1. Illustration of computational mesh. The whole domain is Ω_R with triangulation $\mathcal{T}_{h,R}$. Blue nodes in $\mathcal{T}_{h,R}$ are atoms in $\Lambda^{\mathrm{a,i}}$, and red nodes in $\mathcal{T}_{h,R}$ are continuum degrees of freedom. Ω_R^{a} is the domain and $\mathcal{T}_{h,R}^{\mathrm{a}}$ is the associated triangulation formed by the blue nodes. Ω_R^{c} and $\mathcal{T}_{h,R}^{\mathrm{c}}$ are the respective complement of Ω_R^{a}.

Hence, the space of *coarse-grained* displacements is

$$\mathscr{U}_{h,R} := \big\{ u_h : \Omega_R \to \mathbb{R}^m \,\big|\, \begin{array}{l} u_h \text{ is continuous and p.w. affine w.r.t. } \mathcal{T}_{h,R}, \\ u_h = 0 \text{ on } \partial\Omega_R \end{array} \big\}.$$

Suppose $\mathrm{vor}(\ell)$ is the Voronoi cell associated with a lattice point $\ell \in \Lambda$. For each ℓ, we can choose the associated effective Voronoi cell v_ℓ such that for $\ell \in \Lambda^{\mathrm{a}}$, $v_\ell = \mathrm{vor}(\ell)$ but for $\ell \in \Lambda^{\mathrm{i}}$ the effective Voronoi cell v_ℓ^{i} depends on the geometry of the interface (see [36]). Let $\omega_\ell^{\mathrm{i}} := \dfrac{|v_\ell^{\mathrm{i}}|}{|\mathrm{vor}(\ell)|}$ be the volume ratio of v_ℓ^{i} with resepect to $\mathrm{vor}(\ell)$. For each element $T \in \mathcal{T}_h$ we define the effective volume of T by

$$\omega_T := \frac{|T \backslash (\bigcup_{\ell\in\Lambda^{\mathrm{a}}} \mathrm{vor}(\ell)) \backslash (\bigcup_{\ell\in\Lambda^{\mathrm{i}}} v_\ell^{\mathrm{i}})|}{|\mathrm{vor}(\ell)|}.$$

We note that $\omega_T \neq |T|$ only if $T \notin \mathcal{T}_h^{\mathrm{a}} \bigcup \mathcal{T}_h^{\mathrm{i}}$.

Now we are ready to define the generic a/c coupling energy functional $\mathscr{E}^{\mathrm{h}}$,

$$\mathscr{E}^{\mathrm{h}}(u_h) := \sum_{\ell\in\Lambda^{\mathrm{a}}} V_\ell(u_h) + \sum_{\ell\in\Lambda^{\mathrm{i}}} \omega_\ell^{\mathrm{i}} V_\ell^{\mathrm{i}}(u_h) + \sum_{T\in\mathcal{T}_h} \omega_T W(\nabla u_h|_T) \tag{2.9}$$

$$= \sum_{\ell\in\Lambda} V_\ell^h(I_{\mathrm{a}} u_h) + \sum_{T\in\mathcal{T}_h} \omega_T W(\nabla u_h|_T). \tag{2.10}$$

where V_ℓ^{i} is a modified interface site potential which satisfies certain consistency conditions, ω_ℓ^{i} and ω_T are suitable coefficients. The details will be discussed immediately in Section § 2.4 and references therein.

The goal of the approximate variational problem for a/c coupling is to find

$$u_{h,R} \in \arg\min \big\{ \mathscr{E}^{\mathrm{h}}(u_h) \,\big|\, u_h \in \mathscr{U}_{h,R} \big\}. \tag{2.11}$$

, R in the subscript of $u_{h,R}$ and $\mathscr{U}_{h,R}$ can be omitted if there is no confusion.

2.4. **Consistent Atomistic/Continuum Formulation.** The choice of the interface potential in (2.11) is the key in the formulation of atomistic/continuum coupling methods. In order to demonstrate the a posteriori error estimate for the generic a/c coupling methods, we shall restrict ourselves to the GRAC type methods [36].

2.4.1. *The patch tests.* A key condition that has been widely discussed in the a/c coupling literature is that $\mathscr{E}^{\rm h}$ should exhibit no "ghost forces". We call this condition the *force patch test*, namely,

$$\langle \delta\mathscr{E}^{\rm h}(\mathsf{F}x), v\rangle = 0 \qquad \forall v \in \mathscr{U}_h, \quad \mathsf{F} \in \mathbb{R}^{m\times d}. \tag{2.12}$$

In addition, to guarantee that $\mathscr{E}^{\rm h}$ approximates the atomistic energy $\mathscr{E}^{\rm a}$, it is reasonable to require that the interface potentials satisfy an *energy patch test*

$$V^{\rm i}_\ell(\mathsf{F}x) = V(\mathsf{F}x) \qquad \forall \mathsf{F} \in \mathbb{R}^{m\times d}, \quad \ell \in \Lambda^{\rm i}. \tag{2.13}$$

If an a/c method satisfies the patch test (2.12) and (2.13), it is called a *consistent a/c method*.

2.4.2. *GRAC: Geometric reconstruction based consistent a/c method.* To complete the definition of the consistent a/c coupling energy (2.9) and of the associated variational problem (2.11), we must specify the interface region $\Lambda^{\rm i}$ and the interface site potential. The geometric reconstruction approach was pioneered by Shimokawa *et al* [43], and then modified and extended in [7, 36]. We refer to [37] for details of the implementation of geometric reconstruction based consistent atomistic/continuum (GRAC) energy for multibody potentials with general interaction range and arbitrary interfaces,. The extension of GRAC to 3D is a work in progress [10].

Our prototype implementation of GRAC is for the 2D triangular lattice $\Lambda^{\rm hom} := \mathsf{A}\mathbb{Z}^2$ with

$$\mathsf{A} = \begin{bmatrix} 1 & \cos(\pi/3) \\ 0 & \sin(\pi/3) \end{bmatrix}. \tag{2.14}$$

Let $a_1 = (1,0)^T$, then $a_j = \mathsf{A}^{j-1}a_1$, $j = 1,\dots,6$, are the nearest neighbour directions in $\Lambda^{\rm hom}$.

Given the homogeneous site potential $V\big(Du(\ell)\big)$, we can represent $V^{\rm i}_\ell$ in terms of V. For each $\ell \in \Lambda^{\rm i}, \rho, \varsigma \in \mathcal{R}_\ell$, let $C_{\ell;\rho,\varsigma}$ be free parameters, and define

$$V^{\rm i}_\ell(u_h) := V\Big(\big(\textstyle\sum_{\varsigma\in\mathcal{R}_\ell} C_{\ell;\rho,\varsigma} D_\varsigma u_h(\ell)\big)_{\rho\in\mathcal{R}_\ell}\Big) \tag{2.15}$$

A convenient short-hand notation is

$$V^{\rm i}_\ell(u_h) = V(C_\ell \cdot Du_h(\ell)), \quad \text{where} \quad \begin{cases} C_\ell := (C_{\ell;\rho,\varsigma})_{\rho,\varsigma\in\mathcal{R}_\ell}, & \text{and} \\ C_\ell \cdot Dy := \big(\sum_{\varsigma\in\mathcal{R}_\ell} C_{\ell;\rho,\varsigma} D_\varsigma u\big)_{\rho\in\mathcal{R}_\ell}. \end{cases}$$

we name the parameters $C_{\ell;\rho,\varsigma}$ as the *reconstruction parameters*.

The parameters are chosen so that the resulting energy functional $\mathscr{E}^{\rm h}$ satisfies the energy and force patch tests (2.12) and (2.13). A sufficient (and likely necessary) condition for the energy patch test is that $\mathsf{F}\cdot\mathcal{R}_\ell = C_\ell \cdot (\mathsf{F}\cdot\mathcal{R})$ for all $\mathsf{F} \in \mathbb{R}^{m\times d}$ and $\ell \in \Lambda^{\rm i}$. This is equivalent to

$$\rho = \sum_{\varsigma\in\mathcal{R}_\ell} C_{\ell;\rho,\varsigma}\varsigma, \qquad \forall \ell \in \Lambda^{\rm i}, \quad \rho \in \mathcal{R}_\ell. \tag{2.16}$$

In addition, optimal condition and stabilisation mechanism were proposed in [37] and [28] to improve the accuracy and stability of GRAC scheme.

2.4.3. *Stress formulation.* The stress tensor based formulation can be obtained from the first variation of the energy. For any $u \in \mathscr{U}$, and $u_h \in \mathscr{U}_h$, there exist piecewise constant tensor fields $\sigma^{\mathrm{a}}(u;\cdot) \in \mathrm{P}_0(\mathcal{T}_{\mathrm{a}})^{2\times 2}, \sigma^{\mathrm{c}}(u;\cdot) \in \mathrm{P}_0(\mathcal{T}_{\mathrm{h}})^{2\times 2}$, and $\sigma^{\mathrm{h}}(u;\cdot) \in \mathrm{P}_0(\mathcal{T}_{\mathrm{h}})^{2\times 2}$ which satisfy the following identities

$$\langle \delta\mathscr{E}^{\mathrm{a}}(u), v\rangle = \sum_{T\in\mathcal{T}_{\mathrm{a}}} |T|\sigma^{\mathrm{a}}(u;T) : \nabla_T v, \forall v \in \mathscr{U}, \tag{2.17}$$

$$\langle \delta\mathscr{E}^{\mathrm{c}}(u_h), v_h\rangle = \sum_{T\in\mathcal{T}_{\mathrm{h}}} |T|\sigma^{\mathrm{c}}(u_h;T) : \nabla_T v_h, \forall v_h \in \mathscr{U}_h, \tag{2.18}$$

$$\langle \delta\mathscr{E}^{\mathrm{h}}(u_h), v_h\rangle = \sum_{T\in\mathcal{T}_{\mathrm{h}}} |T|\sigma^{\mathrm{h}}(u_h;T) : \nabla_T v_h, \forall v_h \in \mathscr{U}_h. \tag{2.19}$$

here $\mathcal{T}_{\mathrm{a}}$ is the micro-triangulation induced by the reference lattice Λ. We call σ^{a} an *atomistic stress tensor*, σ^{c} a *continuum stress tensor*, and σ^{h} an *a/c stress tensor*. For the nearest neighbour interactions, we can choose the following atomistic stress tensor, continuum stress tensor, and a/c stress tensor following respectively from the first variations (2.17)-(2.19),

$$\sigma^{\mathrm{a}}(u;T) := \frac{1}{\det \mathsf{A}} \sum_{b=(\ell,\ell+\rho)\in\partial T \bigcap \mathcal{B}} \partial_\rho V_\ell \otimes a_\rho, \tag{2.20}$$

$$\sigma^{\mathrm{c}}(u_h;T) := \partial W(\nabla_T u) = \frac{1}{\det \mathsf{A}} \sum_{j=1}^{6} \partial_j V(\nabla_T u_h) \otimes a_j, \tag{2.21}$$

$$\sigma^{\mathrm{h}}(u_h;T) := \sum_{b=(\ell,\ell+\rho)\in\partial T \bigcap \mathcal{B}} \partial_\rho V_\ell^h(I_{\mathrm{a}} u_h) \otimes a_\rho + \omega_T \sigma^{\mathrm{c}}(u_h;T). \tag{2.22}$$

We call piecewise constant tensor field $\sigma \in \mathrm{P}_0(\mathcal{T})^{2\times 2}$ *divergence free* if

$$\sum_{T\in\mathcal{T}} |T|\sigma(T) : \nabla_T v \equiv 0, \forall v \in (\mathrm{P}_1(\mathcal{T}))^2.$$

By definitions (2.19), it is easy to know that the force patch test condition (2.12) is equivalent to that $\sigma^{\mathrm{h}}(\mathsf{F}x)$ is divergence free for any constant deformation gradient F. The discrete divergence free tensor fields over the triangulation $\mathcal{T}$ can be characterized by the non-conforming Crouzeix-Raviart finite elements [36, 27]. The Crouzeix-Raviart finite element space over $\mathcal{T}$ is defined as

$$N_1(\mathcal{T}) = \{c : \bigcup_{T\in\mathcal{T}} \mathrm{int}(T) \to \mathbb{R} \quad \big| \quad c \text{ is piecewise affine w.r.t. } \mathcal{T}, \text{and continuous in edge midpoints } q_f, \forall f \in \mathcal{F}\}$$

The following lemma in [36] characterizes the discrete divergence-free tensor field.

Lemma 2.2. *A tensor field $\sigma \in \mathsf{P}_0(\mathcal{T})^{2\times 2}$ is divergence free if and only if there exists a constant $\sigma_0 \in \mathbb{R}^{2\times 2}$ and a function $c \in N_1(\mathcal{T})^2$ such that*

$$\sigma = \sigma_0 + \nabla c \mathsf{J}, \qquad \textit{where} \quad \mathsf{J} = \begin{bmatrix} 0 & -1 \\ 1 & 0 \end{bmatrix} \in \mathsf{SO}(2).$$

We also have the following corollary,

Corollary 2.3. *The stress tensors in the definitions* (2.17)-(2.19) *are not unique. Given any stress tensor $\sigma \in \mathsf{P}_0(\mathcal{T})^{2\times 2}$ satisfies one of the definitions* (2.17)-(2.19) ,

where $\mathcal{T}$ is the triangulation in that definition. Let the admissible set be $\mathrm{Adm}(\sigma) := \{\sigma + \nabla \mathsf{c}\mathsf{J}, \mathsf{c} \in \mathrm{N}_1(\mathcal{T})^2\}$*, then any* $\sigma' \in \mathrm{Adm}(\sigma)$ *satisfies the same definition.*

2.4.4. *A Priori Error Estimate.* In the analytical framework proposed in [19, 9], the numerical error can be split into 3 parts: the modeling error due to the discrepancy between the atomistic model and the continuum model at the interface and the finite element edges, the coarsening error due to finite element discretization of the solution space in the continuum region, and the truncation error due to the finite size of the computational domain. It is proven in [9] that there exists a strongly stable solution $u_{h,R}$ to (2.11) and a constant $C^{\mathrm{a-priori}}$for GRAC such that,

$$\|\nabla u_{h,R} - \nabla u\|_{L^2} \leqslant C^{\mathrm{a-priori}}\big(\|hD^2u\|_{\ell^2(\Lambda \bigcap (\Omega_R^{\mathrm{c}}))} + \|Du\|_{\ell^2(\Lambda \setminus B_{R/2})}\big) \tag{2.23}$$

With the generic decay property (2.8), and the following quasi-optimal conditions:

- the radius of the atomistic region $\mathcal{T}_{h,R}^{\mathrm{a}}$ satisfies,
$$\underline{C} R_{\mathrm{a}}^{1+2/d} \leqslant R \leqslant \overline{C} R_{\mathrm{a}}^{1+2/d}, \tag{2.24}$$
- the finite element mesh $\mathcal{T}_{h,R}^{\mathrm{c}}$ is graded so that the mesh size function $h(x) = \mathrm{diam}(T)$ for $T \in \mathcal{T}_{h,R}^{\mathrm{c}}$ satisfies,
$$|h(x)| \leqslant C^{\mathrm{mesh}}\big(\frac{|x|}{R_{\mathrm{a}}}\big)^{\beta}, \text{ with } \beta < \frac{d+2}{2}. \tag{2.25}$$

It holds that there exists a constant $C_0 > 0$, depending on $C^{\mathrm{a-priori}}$, $\underline{C}$, $\overline{C}$, C^{mesh}, and β such that for R sufficiently large,

$$\|\nabla u_{h,R} - \nabla u\|_{L^2} \leqslant C_0 R^{-d/2-1}. \tag{2.26}$$

In particular, when $d = 2$, and when P1 finite elements are used in the continuum region, we have,

$$\|\nabla u_{h,R} - \nabla u\|_{L^2} \leqslant C_0 N^{-1}, \tag{2.27}$$

where N is the overall degrees of freedom.

3. Error Analysis

We present the a posteriori error analysis in this section. In § 3.1, we derive the residual estimate for the consistent GRAC a/c coupling scheme introduced in § 2.4. Then, in § 3.2, we give a lower bound for the stability constant which is computable from the a/c solution u_h. Finally, we put forward the main results Theorem 3.5 and Theorem 3.7 in § 3.3.

3.1. **Residual Estimate.** To be more precise, we restrict ourselves to the case of nearest neighbour multibody interactions, namely, we use the so-called "grac23" method introduced in [36] as the a/c coupling mechanism. We will extend the formulation to general short-range multibody interactions in future works.

For lattice function $u : \Lambda \to \mathbb{R}^m$, we denote its continuous and piecewise affine interpolant with respect to the micro-triangulation $\mathcal{T}_{\mathrm{a}}$ by $I_{\mathrm{a}}u$. Identifying $u = I_{\mathrm{a}}u$, we can define the (piecewise constant) gradient $\nabla u = \nabla I_{\mathrm{a}}u : \mathbb{R}^m \to \mathbb{R}^{m\times d}$ and the spaces of compact and finite energy displacements, respectively, by

$$\mathscr{U}^c := \{u : \Lambda \to \mathbb{R}^m | \mathrm{supp}(\nabla u) \text{ is compact}\}.$$
$$\mathscr{U}^{1,2} := \{u : \Lambda \to \mathbb{R}^m | \nabla u \in L^2\}.$$

It can be shown that that $\mathscr{U}^c$ is dense in $\mathscr{U}^{1,2}$ [9].

The first variation of the atomistic variational problem (2.7) is to find $u \in \mathscr{U}^{1,2}$ such that

$$\langle \delta\mathscr{E}^{\mathrm{a}}(u), v\rangle = 0, \quad \forall v \in \mathscr{U}^{1,2}. \tag{3.1}$$

The first variation of the a/c coupling variational problem (2.11) is to find $u_h \in \mathscr{U}_{h,R}$ such that

$$\langle \delta\mathscr{E}^{\mathrm{h}}(u_h), v_h\rangle = 0, \quad \forall v_h \in \mathscr{U}_{h,R}. \tag{3.2}$$

We introduce the truncation operator T_R as in [9] by first choosing a C^1 cut-off function $\eta(x) = 1$ for $|x| \leqslant 4/6$ and $\eta(x) = 0$ for $|x| \geqslant 5/6$. Define $T_R : \mathscr{U}^{1,2} \to \mathscr{U}_R$ for $R > 0$ by

$$T_R u(\ell) := \eta(\ell/R)(u(\ell) - a_R), \text{ where } a_R := \int_{B_{5R/6}\backslash B_{4R/6}} I_a u(x)\,\mathrm{d}x,$$

where $\mathscr{U}_R$ is defined by

$$\mathscr{U}_R := \{u \in \mathscr{U}^c | u(x) = 0\ \forall x \in \Lambda\backslash\Omega_R\}.$$

The residual R is defined as an operator on $\mathscr{U}^{1,2}$ which is given by

$$\mathsf{R}[v] = \langle \delta\mathscr{E}^{\mathrm{a}}(I_{\mathrm{a}}u_h), v\rangle, \quad \forall v \in \mathscr{U}^{1,2}. \tag{3.3}$$

By (3.2), denote $v_R = T_R v$, and take $v_h = \mathcal{C}_h T_R v : \mathscr{U}^{1,2} \to \mathscr{U}_{h,R}$, where $\mathcal{C}_h : \mathscr{U}_R \to \mathscr{U}_{h,R}$ is the modified Clément operator [4, 47] whose definition will be made clear in the following sections. By (3.2) we can separate the residual into three groups

$$\begin{aligned}\mathsf{R}[v] = \langle \delta\mathscr{E}^{\mathrm{a}}(I_{\mathrm{a}}u_h), v\rangle =& \langle \delta\mathscr{E}^{\mathrm{a}}(I_{\mathrm{a}}u_h), v\rangle - \langle \delta\mathscr{E}^{\mathrm{h}}(u_h), v_h\rangle \\ =& \langle \delta\mathscr{E}^{\mathrm{a}}(I_{\mathrm{a}}u_h), v\rangle - \langle \delta\mathscr{E}^{\mathrm{a}}(I_{\mathrm{a}}u_h), v_R\rangle \\ &+ \langle \delta\mathscr{E}^{\mathrm{a}}(I_{\mathrm{a}}u_h), v_R\rangle - \langle \delta\mathscr{E}^{\mathrm{h}}(u_h), v_R\rangle \\ &+ \langle \delta\mathscr{E}^{\mathrm{h}}(u_h), v_R\rangle - \langle \delta\mathscr{E}^{\mathrm{h}}(u_h), v_h\rangle.\end{aligned}$$

The first group $\mathsf{R}_1 := \langle \delta\mathscr{E}^{\mathrm{a}}(I_{\mathrm{a}}u_h), v\rangle - \langle \delta\mathscr{E}^{\mathrm{a}}(I_{\mathrm{a}}u_h), v_R\rangle$, represents the truncation error; the second group $\mathsf{R}_2 := \langle \delta\mathscr{E}^{\mathrm{a}}(I_{\mathrm{a}}u_h), v_R\rangle - \langle \delta\mathscr{E}^{\mathrm{h}}(u_h), v_R\rangle$ represents the modeling error; and the third group $\mathsf{R}_3 := \langle \delta\mathscr{E}^{\mathrm{h}}(u_h), v_R\rangle - \langle \delta\mathscr{E}^{\mathrm{h}}(u_h), v_h\rangle$ represents the coarsening error. Note that the first variation of the coupling energy is given by

$$\begin{aligned}\langle \delta\mathscr{E}^{\mathrm{h}}(u_h), v_R\rangle :=& \sum_{T\in\mathcal{T}_{\mathrm{h}}} \sigma^{\mathrm{h}}(u_h, T)\Big(\sum_{T'\in\mathcal{T}_{\mathrm{a}}, T'\bigcap T\neq\varnothing} |T\bigcap T'|\nabla v_R\Big) \\ =& \sum_{T\in\mathcal{T}_{\mathrm{h}}} \int_T \sigma^{\mathrm{h}}(u_h, T)\nabla v_R\,\mathrm{d}x \\ =& \sum_{T\in\mathcal{T}_{\mathrm{a}}} |T|\Big(\sum_{T'\in\mathcal{T}_{\mathrm{h}}, T'\bigcap T\neq\varnothing} \frac{|T'\bigcap T|}{|T|}\sigma^{\mathrm{h}}(u_h, T')\Big)\nabla v_R\end{aligned}$$

We will deal with the contribution from those three groups separately in the following subsections.

3.1.1. *Truncation error.* To analyze the truncation error R_1, we need the Lemma 7.3 for the truncation operator T_R in [9], namely, if the radius of the computational domain R is sufficiently large (for example, in the nearest neighbour case, we only need $R > 6$), the following estimates hold

$$\begin{aligned}\|DT_R v - Dv\|_{\ell^2} &\leqslant C^{\mathrm{Tr}}\|Dv\|_{\ell^2(\Lambda\bigcap B_{R/2})} \quad \forall v \in \mathscr{U}^{1,2}, \\ \|DT_R v\|_{\ell^2} &\leqslant C^{\mathrm{Tr}}\|Dv\|_{\ell^2(\Lambda\bigcap B_R)} \quad \forall v \in \mathscr{U}^{1,2},\end{aligned}$$

where C^{Tr} are independent of R.

For any $v \in \mathscr{U}^{1,2}$, the stress-based formulation of the first variation (3.4), the fact that $T_R u(\ell) = u(\ell)$ for $|\ell/R| \leqslant 4/6$, the equivalence of $\|Dv\|_{\ell^2}$ and $\|\nabla v\|_{L^2}$, and Cauchy-Schwarz inequality lead to,

$$\begin{aligned}
|\mathsf{R}_1| &= |\langle \delta\mathscr{E}^{\mathrm{a}}(I_{\mathrm{a}}u_h), v\rangle - \langle \delta\mathscr{E}^{\mathrm{a}}(I_{\mathrm{a}}u_h), T_R v\rangle| \\
&= |\sum_{T\in\mathcal{T}_{\mathrm{a}}} \sigma^{\mathrm{a}}(I_{\mathrm{a}}u_h, T)(\nabla v - \nabla T_R v)| \qquad (3.4)\\
&\leqslant \int_{\Omega_R\setminus B_{R/2}} |\sigma^{\mathrm{a}}(I_{\mathrm{a}}u_h)(\nabla v - \nabla T_R v)|\,\mathrm{d}x \\
&\leqslant \|\sigma^{\mathrm{a}}(I_{\mathrm{a}}u_h)\|_{L^2(\Omega_R\setminus B_{R/2})}\|\nabla v - \nabla T_R v\|_{L^2} \\
&\leqslant C^{\mathrm{Tr}}\|\sigma^{\mathrm{a}}(I_{\mathrm{a}}u_h)\|_{L^2(\Omega_R\setminus B_{R/2})}\|\nabla v\|_{L^2} \qquad (3.5)
\end{aligned}$$

Thus, the truncation error estimator η_T is given by

$$\eta_T(u_h) := C^{\mathrm{Tr}}\|\sigma^{\mathrm{a}}(I_{\mathrm{a}}u_h)\|_{L^2(\Omega_R\setminus B_{R/2})}. \qquad (3.6)$$

3.1.2. *Modeling error.* In the analysis of the modeling error R_2, the stress based formulation leads to,

$$\begin{aligned}
|\mathsf{R}_2| :=& |\langle \delta\mathscr{E}^{\mathrm{a}}(I_{\mathrm{a}}u_h), v_R\rangle - \langle \delta\mathscr{E}^{\mathrm{h}}(u_h), v_R\rangle| \\
=& \Big|\sum_{T\in\mathcal{T}_{\mathrm{a}}} |T|\sigma^{\mathrm{a}}(I_{\mathrm{a}}u_h, T)\nabla v_R - \sum_{T\in\mathcal{T}_{\mathrm{a}}} |T|\Big(\sum_{T'\in\mathcal{T}_{\mathrm{h}}, T'\bigcap T\neq\varnothing} \frac{|T'\bigcap T|}{|T|}\sigma^{\mathrm{h}}(u_h, T')\Big)\nabla v_R\Big| \\
\leqslant& C^{\mathrm{Tr}}\Big\{\sum_{T\in\mathcal{T}_{\mathrm{a}}} |T|\Big[\sigma^{\mathrm{a}}(I_{\mathrm{a}}u_h, T) - \sum_{T'\in\mathcal{T}_{\mathrm{h}}, T'\bigcap T\neq\varnothing} \frac{|T'\bigcap T|}{|T|}\sigma^{\mathrm{h}}(u_h, T')\Big]^2\Big\}^{\frac{1}{2}}\|\nabla v\|_{L^2}.
\end{aligned} \qquad (3.7)$$

As a result, we define the modeling error estimator η_M by,

$$\eta_M(u_h) := C^{\mathrm{Tr}}\Big\{\sum_{T\in\mathcal{T}_{\mathrm{a}}} |T|\Big[\sigma^{\mathrm{a}}(I_{\mathrm{a}}u_h, T) - \sum_{T'\in\mathcal{T}_{\mathrm{h}}, T'\bigcap T\neq\varnothing} \frac{|T'\bigcap T|}{|T|}\sigma^{\mathrm{h}}(u_h, T')\Big]^2\Big\}^{\frac{1}{2}}. \qquad (3.8)$$

3.1.3. *Coarsening error.* For the coarsening error R_3, we first observe that

$$\begin{aligned}
\mathsf{R}_3 :=& \langle \delta\mathscr{E}^{\mathrm{h}}(u_h), v_R\rangle - \langle \delta\mathscr{E}^{\mathrm{h}}(u_h), v_h\rangle, \\
=& \sum_{T\in\mathcal{T}_{\mathrm{h}}} \sigma^{\mathrm{h}}(u_h, T)\Big(\sum_{T'\in\mathcal{T}_{\mathrm{a}}, T'\bigcap T\neq\varnothing} |T\bigcap T'|\nabla v_R\Big) - \sum_{T\in\mathcal{T}_{\mathrm{h}}} |T|\sigma^{\mathrm{h}}(u_h, T)\nabla v_h, \\
=& \sum_{T\in\mathcal{T}_{\mathrm{h}}} \Big(\int_T \sigma^{\mathrm{h}}(u_h, T)\nabla v_R\,\mathrm{d}x - \int_T \sigma^{\mathrm{h}}(u_h, T)\nabla v_h\,\mathrm{d}x\Big), \\
=& \sum_{T\in\mathcal{T}_{\mathrm{h}}} \int_T \sigma^{\mathrm{h}}(u_h, T)(\nabla v_R - \nabla v_h)\,\mathrm{d}x.
\end{aligned} \qquad (3.9)$$

Here, we choose v_h to be the modified Clément interpolation [4, 47] of v_R. For any node $x \in \mathcal{N}_h$ in the triangulation $\mathcal{T}_{\mathrm{h}}$, let ϕ_x be the piecewise linear function with respect to x, and $\omega_x = \mathrm{supp}(\phi_x)$ be the support of ϕ_x. The Clément interpolation operator $\mathcal{C}_h : L^1(\Omega_R) \to V_h$ can be defined as

$$\mathcal{C}_h w = \sum_{x\in\mathcal{N}_h\bigcap \mathrm{Int}(\Omega_R)} w_x\phi_x, \quad \text{where } \ w_x = \frac{\int_{\omega_x} w\phi_x\,\mathrm{d}x}{\int_{\omega_x}\phi_x\,\mathrm{d}x}, \forall x \in \mathcal{N}_h.$$

By definition, $\mathcal{C}_h w$ satisfies the Dirichlet boundary condition. The Clement interpolation possesses the following property [3, 47], for any element $T \in \mathcal{T}_\mathrm{h}$, interior edge $f \in \mathcal{F}_h \bigcap \mathrm{int}(\Omega_\mathrm{R})$,

$$\|w - \mathcal{C}_h w\|_{L^2(T)} \leqslant C_{\mathcal{T}_\mathrm{h}} h_T \|w\|_{H^1(\omega(T))}, \tag{3.10}$$

$$\|w - \mathcal{C}_h w\|_{L^2(f)} \leqslant C'_{\mathcal{T}_\mathrm{h}} h_f^{\frac{1}{2}} \|w\|_{H^1(\omega(f))}. \tag{3.11}$$

where h_T is the diameter of T, h_f is the length of f, the element patch $\omega(T) := \bigcup_{x \in \mathcal{N}_h \bigcap T} \omega_x$, and the edge patch $\omega(f) := \bigcup_{x \in \mathcal{N}_h \bigcap f} \omega_x$. The constants $C_{\mathcal{T}_\mathrm{h}}$ and $C'_{\mathcal{T}_\mathrm{h}}$ depend only on the shape regularity of $\mathcal{T}_\mathrm{h}$.

We also have the stability of the Clément interpolation,

$$\|\nabla \mathcal{C}_h w\|_{L^2(\Omega_R)} \leqslant C''_{\mathcal{T}_\mathrm{h}} \|\nabla w\|_{L^2(\Omega_R)}.$$

where the constant $C''_{\mathcal{T}_\mathrm{h}}$ only depends on the shape regularity of $\mathcal{T}_\mathrm{h}$.

For notational convenience, we suppose that each interior edge $f \in \mathcal{F}_h \bigcap \mathrm{int}(\Omega_R)$ has a prescribed orientation. T_f^+ and T_f^- are the triangles on the left hand side and right hand side of the edge f, ν^+ and ν^- are the associated unit norm vector. The integration by parts of (3.9) leads to,

$$\begin{aligned}
\mathsf{R}_3 &= \sum_{T \in \mathcal{T}_\mathrm{h}} \int_T \sigma^\mathrm{h}(u_h, T)(\nabla v_R - \nabla v_h)\mathrm{d}x \\
&= \sum_{f \in \mathcal{F}_h \bigcap \mathrm{int}(\Omega_R)} \int_f (\sigma^\mathrm{h}(u_h, T_f^+)\nu^+ + \sigma^\mathrm{h}(u_h, T_f^-)\nu^-) \cdot (v_R - v_h)\,\mathrm{d}s \\
&= \sum_{f \in \mathcal{F}_h \bigcap \mathrm{int}(\Omega_R)} [\![\sigma^\mathrm{h}]\!]_f \cdot \int_{f \in \mathcal{F}_h} (v_R - v_h)\,\mathrm{d}s,
\end{aligned}$$

where $[\![\sigma^\mathrm{h}]\!]_f := \sigma^\mathrm{h}(u_h, T_f^+)\nu^+ + \sigma^\mathrm{h}(u_h, T_f^-)\nu^-$ denotes the jump of σ^h across the edge f. Cauchy-Schwarz inequality and the property of Clement interpolation (3.11) give rise to,

$$\begin{aligned}
|\mathsf{R}_3| &\leqslant \sum_{f \in \mathcal{F}_h \bigcap \mathrm{int}(\Omega_R)} |[\![\sigma^\mathrm{h}]\!]_f| h_f^{\frac{1}{2}} \|v_R - v_h\|_{L^2(f)} \\
&\leqslant C'_{\mathcal{T}_\mathrm{h}} \sum_{f \in \mathcal{F}_h \bigcap \mathrm{int}(\Omega_R)} |[\![\sigma^\mathrm{h}]\!]_f| h_f \|\nabla v_R - \nabla v_h\|_{L^2(\omega_f)} \\
&\leqslant C'_{\mathcal{T}_\mathrm{h}} \Big(\sum_{f \in \mathcal{F}_h \bigcap \mathrm{int}(\Omega_R)} (h_f [\![\sigma^\mathrm{h}]\!]_f)^2 \Big)^{\frac{1}{2}} \Big(\sum_{f \in \mathcal{F}_h \bigcap \mathrm{int}(\Omega_R)} \|\nabla v_R - \nabla v_h\|^2_{L^2(\omega_f)} \Big)^{\frac{1}{2}} \\
&\leqslant \sqrt{3} C'_{\mathcal{T}_\mathrm{h}} \Big(\sum_{f \in \mathcal{F}_h \bigcap \mathrm{int}(\Omega_R)} (h_f [\![\sigma^\mathrm{h}]\!]_f)^2 \Big)^{\frac{1}{2}} \|\nabla v_R - \nabla v_h\|_{L^2(\Omega)} \\
&\leqslant \sqrt{3} C^{\mathrm{Tr}} C'_{\mathcal{T}_\mathrm{h}} \Big(\sum_{f \in \mathcal{F}_h \bigcap \mathrm{int}(\Omega_R)} (h_f [\![\sigma^\mathrm{h}]\!]_f)^2 \Big)^{\frac{1}{2}} \|\nabla v\|_{L^2(\Omega)}.
\end{aligned}$$

The coarse-graining error estimator is then defined by,

$$\eta_C(u_h) := \sqrt{3} C^{\mathrm{Tr}} C'_{\mathcal{T}_\mathrm{h}} \Big(\sum_{f \in \mathcal{F}_h} (h_f [\![\sigma^\mathrm{h}]\!]_f)^2 \Big)^{\frac{1}{2}} \tag{3.12}$$

3.1.4. *Residual Estimate.* Combine the estimates for the truncation error, the modeling error and the coarsening error,, we have the following theorem for the residual estimate.

Theorem 3.1. *For $\forall v \in \mathscr{U}^{1,2}$, let u_h be the a/c solution of the residual $\mathsf{R}[v] = \langle \delta\mathscr{E}^{\mathrm{a}}(I_{\mathrm{a}}u_h), v\rangle$ can be bounded by the truncation error (the L^2 norm of the atomistc stress tensor close to the outer boundary), modeling error (the difference of a/c stress tensor and atomistic stress tensor), and the coarsening error (jump of a/c stress tensor across interior edges), namely,*

$$\langle \delta\mathscr{E}^{\mathrm{a}}(I_{\mathrm{a}}u_h), v\rangle \leqslant \big(\eta_T(u_h) + \eta_M(u_h) + \eta_C(u_h)\big)\|\nabla v\|_{L^2}, \tag{3.13}$$

where $\eta_T(u_h)$, $\eta_M(u_h)$ and $\eta_C(u_h)$ are given in (3.6), (3.8) *and* (3.12) *respectively.*

Remark 3.2. All the estimators η_T, η_M and η_C depend on the a/c solution u_h, through discrete stress tensor $\sigma^{\mathrm{h}}(u_h)$ and $\sigma^{\mathrm{a}}(I_{\mathrm{a}}u_h)$. We can define

$$\eta(u_h) := \tilde{\eta}(\sigma^{\mathrm{a}}(I_{\mathrm{a}}u_h), \sigma^{\mathrm{h}}(u_h)) = \eta_T(u_h) + \eta_M(u_h) + \eta_C(u_h). \tag{3.14}$$

By Corollary 2.3, stress tensors $\sigma^{\mathrm{h}}(u_h)$ and $\sigma^{\mathrm{a}}(I_{\mathrm{a}}u_h)$ are unique up to a discrete divergence free tensor, and we denote $\mathrm{Adm}(\sigma^{\mathrm{h}}), \mathrm{Adm}(\sigma^{\mathrm{a}})$ the sets of all possible stress tensors. Therefore the sharp estimate of the residual is

$$\langle \delta\mathscr{E}^{\mathrm{a}}(I_{\mathrm{a}}u_h), v\rangle \leqslant \min_{\mathrm{Adm}(\sigma^{\mathrm{h}}(u_h)),\mathrm{Adm}(\sigma^{\mathrm{a}}(I_{\mathrm{a}}u_h))} \tilde{\eta}(\sigma^{\mathrm{a}}(I_{\mathrm{a}}u_h), \sigma^{\mathrm{h}}(u_h))\|\nabla v\|_{L^2}. \tag{3.15}$$

In Section § 4, we will discuss the details of the implementation of this estimate, which we refer to as "stress tensor correction". □

3.2. **Stability.** In this subsection, we deduce a computable estimate of the a posteriori stability constant. We constrain ourselves in the case of nearest-neighbour interaction with vacancies, and the argument can be extended to finite range interactions. Note that in this case, $\Lambda \subset \Lambda^{\mathrm{hom}}$. We follow the stability analysis in [31] for pair potentials. The main difference is: first, we derive the stability results for the many-body potentials of generic pair functional form (2.4), while in [31] only pair interaction potentials are considered; second, in the a posteriori analysis the stability constant depend on the atomistic Hessian $\delta^2\mathscr{E}^{\mathrm{a}}$ and the a/c solution u_h, which is computable, as opposed to the a priori analysis in [31], the stability constant is related to the a/c Hessian $\delta^2\mathscr{E}^{\mathrm{h}}$ and the atomistic solution u where certain assumptions for u have to be made.

Theorem 3.3. *Suppose that the multi-body interaction potential is of the generic pair functional form* (2.4)*, we have the following results,*

$$\langle \delta^2\mathscr{E}^{\mathrm{a}}(I_a u_h)v, v\rangle \geqslant \gamma(u_h)\|\nabla v\|^2_{L^2(\Omega_R)} \quad \forall v \in \mathscr{U}, \tag{3.16}$$

where the precise definition of $\gamma(u_h)$ will be given as the analysis proceeds.

The proof of Theorem 3.3 can be divided into the following steps:

1. Write $\delta^2\mathscr{E}^{\mathrm{a}}(I_{\mathrm{a}}u_h)$ as a quadratic form with nonuniform coefficients defined on the bonds;
2. Use the perturbation argument (3.22), (3.23) to bound $\delta^2\mathscr{E}^{\mathrm{a}}$ by quantities from a uniform deformation;
3. Define the so-called vacancy stability index (3.26) to further bound $\delta^2\mathscr{E}^{\mathrm{a}}$ for lattice with defects by the second variation for uniformly deformed lattice;
4. The stability constant can be obtained through an optimization procedure.

Recall that from (2.2) that $\mathcal{B}$ is the collection of all the nearest neighbour bonds in the reference lattice Λ. Here we define

$$\mathbb{B} := \{(\ell, \ell+\rho) : \ell \in \Lambda^{\rm hom}, \rho \in \mathcal{R}_\ell\} \tag{3.17}$$

to be the collection of all the nearest neighbour bonds in the homogeneous reference lattice $\Lambda^{\rm hom}$. In the following analysis of this section, we use u to denote $I_a u_h$, and Ω to denote Ω_R in order to keep the notations simple.

3.2.1. *Second variation of the energy.* Using the generic pair functional form multi-body interaction potential (2.4) and Remark 2.1, we write out the second variation of the atomistic energy $\mathscr{E}^{\rm a}(u) = \sum_{\ell\in\Lambda} V(|Du(\ell)|)$ as

$$\begin{aligned}
\langle \delta^2 \mathscr{E}^{\rm a}(u)v, v\rangle =& \sum_{\ell\in\Lambda}\sum_{\rho\varsigma\in\mathcal{R}_\ell} \partial_{\rho\varsigma} V(|Du(\ell)|)(D_\rho v(\ell))^T \big(\frac{D_\rho u(\ell)}{|D_\rho u(\ell)|}\otimes\frac{D_\varsigma u(\ell)}{|D_\varsigma u(\ell)|}\big)(D_\varsigma v(\ell)) \\
&+ \sum_{\ell\in\Lambda}\sum_{\rho\in\mathcal{R}_\ell} \frac{\partial_\rho V(|Du(\ell)|)}{|D_\rho u(\ell)|}(D_\rho v(\ell))^T\big(\mathsf{I} - \frac{D_\rho u(\ell)}{|D_\rho u(\ell)|}\otimes\frac{D_\rho u(\ell)}{|D_\rho u(\ell)|}\big) D_\rho v(\ell) \\
=& \sum_{\ell\in\Lambda}\sum_{\rho\in\mathcal{R}_\ell} \frac{\partial_{\rho\rho} V(|Du(\ell)|)}{|D_\rho u(\ell)|^2}(D_\rho u(\ell)\cdot D_\rho v(\ell))^2 \\
&+ \sum_{\ell\in\Lambda}\sum_{\rho,\varsigma\in\mathcal{R}_\ell,\rho\neq\varsigma} \frac{\partial_{\rho\varsigma} V(|Du(\ell)|)}{|D_\rho u(\ell)||D_\varsigma u(\ell)|}(D_\rho u(\ell)\cdot D_\rho v(\ell))(D_\varsigma u(\ell)\cdot D_\varsigma v(\ell)) \\
&+ \sum_{\ell\in\Lambda}\sum_{\rho\in\mathcal{R}_\ell} \frac{\partial_\rho V(|Du(\ell)|)}{|D_\rho u(\ell)|^3}|D_\rho u(\ell)\times D_\rho v(\ell)|^2,
\end{aligned} \tag{3.18}$$

where $\partial_\rho V(|Du(\ell)|)$ represents the first order partial derivatives of $V(|Du(\ell)|)$ with respect to $|D_\rho u(x)|$, and $\partial_{\rho\varsigma} V(|Du(\ell)|)$ represents the second order partial derivatives with respect to $|D_\rho u(\ell)|$ and $|D_\varsigma u(\ell)|$, I is the identity matrix, and $a\times b = a_1b_2 - a_2b_1$. We have also used the identity

$$\begin{aligned}
h_1^T(\frac{r_1}{|r_1|}\otimes\frac{r_2}{|r_2|})h_2 &= (h_1\cdot\frac{r_1}{|r_1|})(h_2\cdot\frac{r_2}{|r_2|}), \\
\text{and } h^T(\mathsf{I} - \frac{r}{|r|}\otimes\frac{r}{|r|})h &= |h\times\frac{r}{|r|}|^2.
\end{aligned} \tag{3.19}$$

For nearest neighbour interactions, $|\mathcal{R}(\ell)| \leqslant 6$, we define

$$\begin{aligned}
&C^1_{\ell,\rho} = \frac{\partial_{\rho\rho}V(Du(\ell))}{|D_\rho u(\ell)|^2}, \quad C^2_{\ell,\rho} = 0 \wedge \min_{\varsigma,\varsigma\neq\rho}\frac{\partial_{\rho\varsigma}V(Du(\ell))}{|D_\rho u(\ell)||D_\varsigma u(\ell)|}, \\
&C_{\ell,\rho} = \min_\ell(C^1_{\ell,\rho} - 5C^2_{\ell,\rho}), \quad C^\perp_{\ell,\rho} = \frac{\partial_\rho V(Du(\ell))}{|D_\rho u(\ell)|^3}.
\end{aligned}$$

Apply Cauchy-Schwarz inequality to (3.18), we obtain the following estimate,

$$\begin{aligned}\langle \delta^2 \mathscr{E}^{\mathrm{a}}(u)v, v\rangle \geqslant & \sum_{\ell\in\Lambda}\sum_{\rho\in\mathcal{R}_\ell} C_{\ell,\rho}|D_\rho u(\ell)\cdot D_\rho v(\ell)|^2 + \sum_{\ell\in\Lambda}\sum_{\rho\in\mathcal{R}_\ell} C^\perp_{\ell,\rho}|D_\rho u(\ell)\times D_\rho v|^2\\ =&\sum_{b\in\mathcal{B}} C_b|D_b u(\ell)\cdot D_b v(\ell)|^2 + \sum_{b\in\mathcal{B}} C^\perp_b|D_b u(\ell)\times D_b v(\ell)|^2\\ \geqslant& C\sum_{b\in\mathcal{B}}|D_b u(\ell)\cdot D_b v(\ell)|^2 + C^\perp\sum_{b\in\mathcal{B}}|D_b u(\ell)\times D_b v(\ell)|^2\\ =& C\sum_{b\in\mathcal{B}}\int_b |D_b u\cdot\nabla_b v|^2\,\mathrm{db} + C^\perp\sum_{b\in\mathcal{B}}\int_b |D_b u\times\nabla_b v|^2\,\mathrm{db}. \end{aligned} \tag{3.20}$$

where $C_b := C_{\ell,\rho}$ and $C^\perp_b := C^\perp_{\ell,\rho}$ for $b = (\ell, \ell+\rho)$, $C^{(\perp)} := \min_{b\in\mathcal{B}} C^{(\perp)}_b$ (here we use $C^{(\perp)}$ to denote both C and $C^\perp$ for brevity). We have also used the fact that for nearest neighbour interactions, $D_b v = \nabla_b v(\ell)$, $\forall \ell \in \mathrm{int(b)}$, and $D_b u$ is a constant for each $b \in \mathcal{B}$.

3.2.2. *The perturbation argument.* Our next task is to obtain the estimates,

$$C\sum_{b\in\mathcal{B}}\int_b |D_b u\cdot\nabla_b v|^2\,\mathrm{db} \geqslant c\|\nabla v\|^2_{L^2(\Omega)},\ \text{and}\ C^\perp\sum_{b\in\mathcal{B}}\int_b |D_b u\times\nabla_b v|^2\,\mathrm{db} \geqslant c^\perp\|\nabla v\|^2_{L^2(\Omega)}, \tag{3.21}$$

for some $c > 0$ and $c^\perp$ (which could be negative).

(3.21) is not straighforward since $D_b u$ varies on each $b \in \mathcal{B}$. To tackle this issue, we use the following perturbation results from Lemma 6.3 of [31]. For $g \in \mathbb{R}^2$, $b \in \mathcal{B}$, and $\alpha > 0$, we have

$$\left||D_b u\cdot g|^2 - |\mathsf{B}\rho_b\cdot g|^2\right| \leqslant \alpha|\mathsf{B}\rho_b\cdot g|^2 + (1+\frac{1}{\alpha})\Delta^2|\rho_b|^2|\mathsf{B}^T g|^2, \tag{3.22}$$

$$\text{and}\ \left||D_b u\times g|^2 - |\mathsf{B}\rho_b\times g|^2\right| \leqslant \alpha^\perp|\mathsf{B}\rho_b\times g|^2 + (1+\frac{1}{\alpha^\perp})\Delta^2|\rho_b|^2|\mathsf{B}^T g^\perp|^2. \tag{3.23}$$

where ρ_b is the direction vector of b, $\mathsf{B} \in \mathbb{R}^{2\times 2}$ is fixed, and $\Delta = \max_{T\in\mathcal{T}} \|\mathsf{B}^{-1}\nabla u|_T - \mathsf{I}\|$, $g^\perp$ is obtained by $\pi/2$ counterclockwise rotation of g.

Given u, Δ and B can be computed. We will choose $\alpha^{(\perp)}$ in the subsequent analysis to keep the estimate of the stability constant sharp. Applying(3.22) and (3.23) to (3.20), taking the same α and $\alpha^\perp$ for each bond $b \in \mathcal{B}$ and using the fact

that $|\rho_b| = 1$, we obtain

$$\begin{aligned}
&C\sum_{b\in\mathcal{B}}\int_b |D_b u\cdot\nabla_b v|^2\,\mathrm{d}b + C^\perp\sum_{b\in\mathcal{B}}\int_b |D_b u\times\nabla_b v|^2\,\mathrm{d}b\\
\geqslant& C\sum_{b\in\mathcal{B}}\int_b |\mathsf{B}\rho_b\cdot\nabla_b v|^2\,\mathrm{d}b + C^\perp\sum_{b\in\mathcal{B}}\int_b |\mathsf{B}\rho_b\times\nabla_b v|^2\,\mathrm{d}b\\
&-\Big(\alpha|C|\sum_{b\in\mathcal{B}}\int_b |\mathsf{B}\rho_b\cdot\nabla_b v|^2\,\mathrm{d}b + \alpha^\perp|C^\perp|\sum_{b\in\mathcal{B}}\int_b |\mathsf{B}\rho_b\times\nabla_b v|^2\,\mathrm{d}b\\
&+\Delta^2 C(1+\frac{1}{\alpha})\sum_{b\in\mathbb{B}}\int_b |\mathsf{B}^T\nabla_b v|^2\,\mathrm{d}b + \Delta^2 C^\perp(1+\frac{1}{\alpha^\perp})\sum_{b\in\mathbb{B}}\int_b |\mathsf{B}^T\nabla_b v^\perp|^2\,\mathrm{d}b\Big)\\
=&\tilde{C}\sum_{b\in\mathcal{B}}\int_b |\rho_b\cdot\nabla_b v_{\mathsf{B}}|^2\,\mathrm{d}b + \tilde{C}^\perp\sum_{b\in\mathcal{B}}\int_b |\rho_b\times\nabla_b v_{\mathsf{B}}|^2\,\mathrm{d}b\\
&-\Big(\Delta^2 C(1+\frac{1}{\alpha})\sum_{b\in\mathbb{B}}\int_b |\mathsf{B}^T\nabla_b Ev|^2\,\mathrm{d}b + \Delta^2 C^\perp(1+\frac{1}{\alpha^\perp})\sum_{b\in\mathbb{B}}\int_b |\mathsf{B}^T\nabla_b Ev^\perp|^2\,\mathrm{d}b\Big)
\end{aligned}$$

where $\tilde{C}^{(\perp)} := C^{(\perp)} - \alpha|C^{(\perp)}|$, we have used $\mathsf{B}^T\nabla_b v = \nabla_b\mathsf{B}^T v$, $\mathsf{B}\rho_b\cdot\nabla_b v = \rho_b\cdot\mathsf{B}^T\nabla_b v$, and $v_{\mathsf{B}} := \mathsf{B}^T v$. Ev is the extension of v from Λ to the vacancy sites defined in the Appendix § 6.1, it is clear that $Ev^\perp = (Ev)^\perp$.

Let

$$\langle\tilde{H}v, v\rangle := \tilde{C}\sum_{b\in\mathcal{B}}\int_b |\rho_b\cdot\nabla_b v_{\mathsf{B}}|^2\,\mathrm{d}b + \tilde{C}^\perp\sum_{b\in\mathcal{B}}\int_b |\rho_b\times\nabla_b v_{\mathsf{B}}|^2\,\mathrm{d}b$$

and

$$\begin{aligned}
\langle\tilde{\mathcal{L}}^{(\perp)}v, v\rangle :&= C^{(\perp)}(1+\frac{1}{\alpha^{(\perp)}})\sum_{b\in\mathbb{B}}\int_b |\mathsf{B}^T\nabla_b Ev^{(\perp)}|^2\,\mathrm{d}b\\
&= \tilde{L}^{(\perp)}\|\nabla(\mathsf{B}^T Ev^{(\perp)})\|^2_{L^2(\Omega)}.
\end{aligned}\tag{3.24}$$

where $\tilde{L}^{(\perp)} = \dfrac{3}{\det\mathsf{A}_6}(1+\dfrac{1}{\alpha^{(\perp)}})C^{(\perp)}$. (3.24) is due to the application of the so-called bond-density lemma with respect to Dirichlet boundary conditions [40, Lemma 4.5]. This leads to the following error estimate,

$$\langle\delta^2\mathscr{E}^{\mathrm{a}}(u)v, v\rangle \geqslant \langle\tilde{H}(u)v, v\rangle - \Delta^2(\tilde{L}\|\nabla(\mathsf{B}^T Ev)\|^2_{L^2(\Omega)} + \tilde{L}^\perp\|\nabla(\mathsf{B}^T Ev^\perp)\|^2_{L^2(\Omega)}) \tag{3.25}$$

3.2.3. *Vacancy stability index.* Then we introduce the vacancy stability index κ as

$$\kappa(\mathbb{V}) = \max\Big\{k>0 : \Phi_{\mathcal{B}}(u)\geqslant k\Phi_{\mathbb{B}}(Eu),\ \forall u\in\mathscr{U}\Big\}. \tag{3.26}$$

Since $\tilde{C} > 0$ and $\tilde{C}^\perp$ might be negative, we define the constants

$$\bar{C}^{(\perp)} := \min(\tilde{C}^{(\perp)}, \kappa\tilde{C}^{(\perp)}). \tag{3.27}$$

We can further estimate (3.25) by

$$\begin{aligned}
\langle\mathcal{H}v, v\rangle \geqslant&\bar{C}\sum_{b\in\mathbb{B}}\int_b |\rho_b\cdot\nabla_b(E\mathsf{B}^T v)|^2\,\mathrm{d}b + \bar{C}^\perp\sum_{b\in\mathbb{B}}\int_b |\rho_b\times\nabla_b(E\mathsf{B}^T v)|^2\,\mathrm{d}b\\
&-\Delta^2(\tilde{L}\|\nabla(\mathsf{B}^T Ev)\|^2_{L^2(\Omega)} + \tilde{L}^\perp\|\nabla(\mathsf{B}^T Ev^\perp)\|^2_{L^2(\Omega)}).
\end{aligned}\tag{3.28}$$

3.2.4. *Stability of the homogenous lattice.* We now need the stability estimates for homogeneous lattice. Let

$$\langle \bar{\mathcal{H}} v, v\rangle = \bar{C}\sum_{b\in\mathbb{B}}\int_b |\rho_b\cdot\nabla_b(E\mathsf{B}^T v)|^2\,\mathrm{db} + \bar{C}^{\perp}\sum_{b\in\mathbb{B}}\int_b |\rho_b\times\nabla_b(E\mathsf{B}^T v)|^2\,\mathrm{db}. \tag{3.29}$$

By Lemma 6.4 of [31], we have

$$\langle \bar{\mathcal{H}} v, v\rangle \geqslant \bar{\gamma}\|\nabla E\mathsf{B}^T v\|^2_{L^2(\Omega)}. \tag{3.30}$$

where $\bar{\gamma} := \min(\frac{3}{4}\bar{c} + \frac{9}{4}\bar{c}^{\perp}, \frac{9}{4}\bar{c} + \frac{3}{4}\bar{c}^{\perp})$, and $\bar{c}^{(\perp)} = \dfrac{3}{\det \mathsf{A}_6}\bar{C}^{(\perp)}$.

Furthermore, by the inequality (6.3) for the extension operator E, we can estimate the stability of atomistic Hessian (3.28) by,

$$\langle \delta^2\mathscr{E}^{\mathrm{a}}(u)v, v\rangle \geqslant \gamma(u)\|\nabla v\|^2_{L^2(\Omega)}. \tag{3.31}$$

where

$$\gamma(u) = \frac{1}{3}\|B^{-1}\|_F^{-2}\bar{\gamma} - \Delta^2\|B\|_F^2(\tilde{L} + \tilde{L}^{\perp}). \tag{3.32}$$

3.2.5. *Numerical Justification.* Tracing back the derivation of the stability constant γ, the only free parameters are α, $\alpha^{\perp}$. Consequently, we can find γ by an optimization procedure with respect to α and $\alpha^{\perp}$.

We justify our estimation of the stability of the atomistic Hessian numerically. We apply the same EAM potential as in § 4.2. We take isotropic stretch S and shear loading γ_{II} by setting

$$\mathsf{B} = \begin{pmatrix} 1+\mathrm{S} & \gamma_{II} \\ 0 & 1+\mathrm{S}\end{pmatrix}\cdot\mathsf{F}_0,$$

where $\mathsf{F}_0 \propto \mathrm{I}$ minimizing W. The results are listed in the following tables, where λ stands for the smallest eigenvalue of atomistic Hessian, and γ represents the optimal estimate of the stability constant.

number of vacancies	0	1	2
λ	17.436	14.107	12.905
γ	5.284	2.206	1.451

TABLE 1. In this example $\mathrm{S} = \gamma_{II} = 0$. The degrees of freedom of the atomistic model is about 3×10^4.

number of vacancies	0	1	2
λ	11.125	9.809	8.946
γ	3.159	0.468	-0.258

TABLE 2. In this example $\mathrm{S} = \gamma_{II} = 0.03$. The degrees of freedom of the atomistic model is about 3×10^4.

From the numerical results, our estimates indeed give lower bound of the minimal eigenvalue of atomistic Hessian, however, the estimate may become negative when the deformation and number of vacancy sites increase. To compute Δ, B and then the stability constant, we used CVX, a package for specifying and solving convex programs [13].

3.3. **Main results.** We present the main theorems for the a posteriori errors in H^1 norm and energy separately in this section.

3.3.1. *A Posteriori Error Estimates in H^1 norm.* Here we propose a rigorous justification of the H^1-a posteriori error estimate. The proof makes use of a quantitative version of the inverse function theorem [19].

Lemma 3.4. *Let X be a Hilbert space, $w_0 \in X$, R, $M > 0$, and $E \in C^2(B_R^X(\omega_0))$ with Lipschitz continuous Hessian, $\|\delta^2 E(x) - \delta^2 E(y)\|_{L(X,X^*)} \leqslant M\|x-y\|_X$ for $x, y \in B_R^X(\omega_0)$. Suppose, moreover, that there exists constants c, $r > 0$, such that*

$$\langle \delta^2 E(w_0)v, v\rangle \geqslant c\|v\|_X^2, \quad , \|\delta E(w_0)\|_{X^*} \leqslant r, \quad \text{and } 2Mrc^{-2} < 1. \tag{3.33}$$

Then there exists a unique $\bar{w} \in B_{2rc^{-1}}^X(w_0)$ with $\delta E(\bar{w}) = 0$ and

$$\langle \delta^2 E(\bar{w})v, v\rangle \geqslant (1 - 2Mrc^{-2})c\|v\|_X^2.$$

Take $X = \mathscr{U}^h$, ω_0 as the a/c solution u_h of (3.2), and M as the Lipschitz constant of $\delta^2\mathscr{E}^{\mathrm{a}}$. Combine the residue estimate in Theorem 3.1, stability estimate in Theorem 3.3, and inverse function theorem Lemma 3.4, we have the following theorem for the a posteriori existence and error estimate.

Theorem 3.5. *Let $\eta(u_h)$ be the residual defined in (3.14), $\gamma(u_h)$ be the stability constant defined in (3.32), and M be the Lipschitz constant of $\delta^2\mathscr{E}^{\mathrm{a}}$. Under the assumption that $2M\eta(u_h) < \gamma(u_h)^2$, there exists a unique $u \in \mathscr{U}^{1,2}$ which solves the atomistic variational problem (3.1), and satisfies the following error bound,*

$$\|\nabla I_{\mathrm{a}} u_h - \nabla u\|_{L^2} \leqslant 2\frac{\eta(u_h)}{\gamma(u_h)}, \tag{3.34}$$

and the strong stability condition,

$$\langle \delta^2 E(u)v, v\rangle \geqslant \big(1 - 2\frac{M\eta(u_h)}{\gamma(u_h)^2}\big)\gamma(u_h)\|v\|_{L^2}^2, \quad \forall v \in \mathscr{U}^{1,2}. \tag{3.35}$$

Remark 3.6. Alternatively, the a posteriori error estimate can be deduced by the following argument in [35], but we need to assume the existence of the atomistic solution u and the closeness of u to $I_{\mathrm{a}}u_h$. By mean value theorem, there exists $\theta \in \mathrm{conv}\{u, I_{\mathrm{a}}u_h\}$ such that

$$\begin{aligned}\langle \delta^2\mathscr{E}^{\mathrm{a}}(\theta)v, v\rangle &= \langle \delta\mathscr{E}^{\mathrm{a}}(I_{\mathrm{a}}u_h), v\rangle - \langle \delta\mathscr{E}^{\mathrm{a}}(u), v\rangle \\ &= \langle \delta\mathscr{E}^{\mathrm{a}}(I_{\mathrm{a}}u_h), v\rangle \\ &\leqslant \eta(u_h)\|\nabla v\|_{L^2(\Omega)}.\end{aligned} \tag{3.36}$$

Combine the coercivity of $\mathscr{E}^{\mathrm{a}}$ at $I_{\mathrm{a}}u_h$,

$$\langle \delta^2\mathscr{E}^{\mathrm{a}}(I_{\mathrm{a}}u_h)v, v\rangle \geqslant \gamma(u_h)\|\nabla v\|_{L^2}^2,$$

and the Lipschitz continuity (Fréchet differentiability) of $\delta^2\mathscr{E}^{\mathrm{a}}$, we obtain that

$$\begin{aligned}\langle \delta^2\mathscr{E}^{\mathrm{a}}(\theta)v, v\rangle &\geqslant \langle \delta^2\mathscr{E}^{\mathrm{a}}(I_{\mathrm{a}}u_h)v, v\rangle - M\|u - I_{\mathrm{a}}u_h\|_{W^{1,\infty}}\|\nabla v\|_{L^2}^2 \\ &\geqslant (\gamma(u_h) - M\|u - I_{\mathrm{a}}u_h\|_{W^{1,\infty}})\|\nabla v\|_{L^2}^2\end{aligned} \tag{3.37}$$

Let $v = u - I_{\mathrm{a}}u_h$ in (3.37), using (3.36), we have

$$\|\nabla u - \nabla I_{\mathrm{a}}u_h\|_{L^2} \leqslant \frac{2\eta(u_h)}{\gamma(u_h)} \tag{3.38}$$

if the closeness assumption $\|\nabla u_h - \nabla u\|_{L^\infty} \leqslant \dfrac{\gamma(u_h)}{2M}$ remains true.

□

3.3.2. *A Posteriori Error Estimate for the Energy.* Total energy is an important physical quantity to be approximated in practice. In this section, we will derive an estimate for the energy difference $\mathscr{E}^{\mathrm{a}}(u)-\mathscr{E}^{\mathrm{h}}(u_h)$. The energy difference can be split into the sum of $\mathscr{E}^{\mathrm{a}}(u) - \mathscr{E}^{\mathrm{a}}(I_{\mathrm{a}}u_h)$ and $\mathscr{E}^{\mathrm{a}}(I_{\mathrm{a}}u_h) - \mathscr{E}^{\mathrm{h}}(u_h)$, thus

$$|\mathscr{E}^{\mathrm{a}}(u) - \mathscr{E}^{\mathrm{h}}(u_h)| \leqslant |\mathscr{E}^{\mathrm{a}}(u) - \mathscr{E}^{\mathrm{a}}(I_{\mathrm{a}}u_h)| + |\mathscr{E}^{\mathrm{a}}(I_{\mathrm{a}}u_h) - \mathscr{E}^{\mathrm{h}}(u_h)| \tag{3.39}$$

For the first part, use the fact that $\mathscr{E}^{\mathrm{a}}$ is twice differentiable along the segment $\{(1-s)u + sI_{\mathrm{a}}u_h | s \in (0,1)\}$, we obtain

$$\begin{aligned}
|\mathscr{E}^{\mathrm{a}}(u) - \mathscr{E}^{\mathrm{a}}(I_{\mathrm{a}}u_h)| &= |\int_0^1 \langle \delta\mathscr{E}^{\mathrm{a}}((1-s)u + sI_{\mathrm{a}}u_h), u - u_h\rangle \mathrm{d}s| \\
&= |\int_0^1 \langle \delta\mathscr{E}^{\mathrm{a}}((1-s)u + sI_{\mathrm{a}}u_h) - \delta\mathscr{E}^{\mathrm{a}}(u), u - I_{\mathrm{a}}u_h\rangle \mathrm{d}s| \\
&\leqslant M\|Du - DI_{\mathrm{a}}u_h\|_{\ell^2}^2 \\
&\leqslant M\|\nabla u - \nabla I_{\mathrm{a}}u_h\|_{L^2}.
\end{aligned} \tag{3.40}$$

which can be further estimated by Theorem 3.5, the constant M is the Lipschitz constant of $\delta^2\mathscr{E}^{\mathrm{a}}$ which does not depend on u_h.

For the second part, let $\mu_E(u_h) := \mathscr{E}^{\mathrm{a}}(I_{\mathrm{a}}u_h) - \mathscr{E}^{\mathrm{h}}(u_h)$. Noticing that $V_\ell = V$ when $T \bigcap \Lambda^{\mathrm{a}} = \varnothing$, we can rewrite $\mathscr{E}^{\mathrm{a}}$ in the site based form,

$$\mathscr{E}^{\mathrm{a}}(I_{\mathrm{a}}u_h) = \sum_{T\in\mathcal{T}_{\mathrm{a}}} \frac{1}{6} \sum_{\ell\in T\bigcap\Lambda} V_\ell(I_{\mathrm{a}}u_h).$$

Moreover, given $\mathscr{E}^{\mathrm{h}}$ of the form (2.9), assuming for simplicity $\omega_\ell^{\mathrm{i}} = 1$, and $\mathcal{T}_h^{\mathrm{i}}$ is a few layers of atomistic micro-triangulation around the $\mathcal{T}_h^{\mathrm{a}}$, which is actually the case for the implementation in [36], we can rewrite $\mathscr{E}^{\mathrm{h}}$ as follows,

$$\begin{aligned}
\mathscr{E}^{\mathrm{h}}(u_h) = &\sum_{T\in\mathcal{T}_h^{\mathrm{a}}} \frac{1}{6} \sum_{\ell\in T\bigcap\Lambda^{\mathrm{a}}} V_\ell(I_{\mathrm{a}}u_h) + \sum_{T\in\mathcal{T}_h^{\mathrm{a}}} \frac{1}{6} \sum_{\ell\in T\bigcap\Lambda^{\mathrm{i}}} V_\ell^{\mathrm{i}}(I_{\mathrm{a}}u_h) + \\
&\sum_{T\in\mathcal{T}_h^{\mathrm{i}}\bigcap\mathcal{T}_h^{\mathrm{c}}} \Big\{ \sum_{\ell\in T\bigcap\Lambda^{\mathrm{i}}} \frac{1}{6} \sum_{\ell\in T} V_\ell^{\mathrm{i}}(I_{\mathrm{a}}u_h) + (1 - \frac{\#\{\ell\in T\bigcap\Lambda^{\mathrm{i}}\}}{3})|T|W(\nabla I_{\mathrm{a}}u_h) \Big\} + \\
&\sum_{T\in\mathcal{T}_{\mathrm{h}}^{\mathrm{c}}\setminus\mathcal{T}_h^{\mathrm{i}}} \sum_{T'\in\mathcal{T}_{\mathrm{a}}, T'\bigcap T\neq\varnothing} |T\bigcap T'|W(\nabla I_{\mathrm{a}}u_h).
\end{aligned}$$

Hence μ_E can be expanded as,

$$\begin{aligned}\mu_E(u_h) = &\sum_{T\in\mathcal{T}_h^{\mathrm{a}}}\frac{1}{6}\sum_{\ell\in T\bigcap\Lambda^{\mathrm{i}}}\big(V_\ell(I_{\mathrm{a}}u_h)-V_\ell^{\mathrm{i}}(I_{\mathrm{a}}u_h)\big)+\\ &\sum_{T\in\mathcal{T}_h^{\mathrm{i}}\bigcap\mathcal{T}_h^{\mathrm{c}}}\Big\{\sum_{\ell\in T\bigcap\Lambda^{\mathrm{i}}}\frac{1}{6}\sum_{\ell\in T}V_\ell(I_{\mathrm{a}}u_h)-\sum_{\ell\in T\bigcap\Lambda}\frac{1}{6}\sum_{\ell\in T}V_\ell^{\mathrm{i}}(I_{\mathrm{a}}u_h)+\\ &(1-\frac{\#\{\ell\in T\bigcap\Lambda^{\mathrm{i}}\}}{3})|T|W(\nabla I_{\mathrm{a}}u_h)\Big\}+\\ &\sum_{T\in\mathcal{T}_h^{\mathrm{c}}\setminus\mathcal{T}_h^{\mathrm{i}}}\sum_{T'\in\mathcal{T}_{\mathrm{a}},T'\bigcap T\neq\varnothing}\frac{|T\bigcap T'|}{|T'|}(\frac{1}{6}\sum_{\ell\in T'}V_\ell(I_{\mathrm{a}}u_h)-W(\nabla u_h)).\end{aligned}\tag{3.41}$$

We note that the summand in the last term, that is summed over $T\in\mathcal{T}_{\mathrm{h}}^{\mathrm{c}}$, is nonzero only if $\omega(T')\bigcap\partial T\neq\varnothing$, therefore can be rewritten as

$$\sum_{T\in\mathcal{T}_{\mathrm{h}}^{\mathrm{c}}}\sum_{T'\in\mathcal{T}_{\mathrm{a}},\omega(T')\bigcap\partial T\neq\varnothing}\frac{|T\bigcap T'|}{2|T'|}(\frac{1}{3}\sum_{\ell\in T}V(DI_{\mathrm{a}}u_h(\ell))-V(\nabla I_{\mathrm{a}}u_h\rho)).$$

We hence have the following theorem,

Theorem 3.7. *Given the same condition as in Theorem 3.5, the difference of the energy can be bound by the following inequality,*

$$|\mathscr{E}^{\mathrm{a}}(u)-\mathscr{E}^{\mathrm{h}}(u_h)|\leqslant C^E(\eta(u_h))^2+|\mu_E(u_h)|.$$

where $C^E=\frac{2M}{\gamma(u_h)}$, $\eta(u_h)$ *and* $\mu_E(u_h)$ *are defined in* (3.14) *and* (3.41) *respectively.*

4. Adaptive Algorithms and Numerical Experiments

In this section, we propose an adaptive mesh refinement algorithm based on the a posteriori error estimates in Theorem 3.5 and Theorem 3.7. Numerical experiments show that our algorithm achieves an optimal convergence rate in terms of accuracy vs. the number of the degrees of freedom, which is consistent with the a priori error estimates.

4.1. Adaptive mesh refinement algorithm.

We have constructed the residue based error estimators η_M, η_C, η_T in § 3.1 and μ_E in § 3.3.2. Our goal is to design adaptive refinement algorithms based on those estimators. The algorithm follows the usual Solve-Mark-Refine-Estimate procedure. However, compared to adaptive mesh refinement algorithms for the numerical solution for continuous PDEs, the major difference is two-fold:

- The errors η_M, η_C and η_T depend on u_h through stress tensors σ^{h} and σ^{a} which are not unique. Therefore, we can minimize the error estimator with respect to all the possible stress tensors, and we call this procedure "stress tensor correction".
- The modeling error η_M results from the inconsistency of the atomistic model and the continuum model at the interface and finite element edges. In particular, when the interface error is large, we need to enlarge the atomistic domain Ω^{a}, and adjust the triangulation in the continuum domain such that the mesh in the continuum region aligns with the micro-triangulation $\mathcal{T}_{\mathrm{a}}$ close to the interface, such that the overall triangulation maintains good quality.

- The truncation error η_T is introduced by the truncation of an infinite lattice to a finite domain. If the size of the computation domain is fixed, we shall see the saturation of the numerical error when the number of degrees of freedom N is increased. Therefore, if η_T is dominant in the overall error η, we can increase the domain size in order to achieve the optimal convergence rate.

Corresponding to those differences, we need new ingredients for the implementation of the adaptive algorithm.

4.1.1. *Stress tensor correction.* By Theorem 3.1 and Remark 3.2, the error estimators η_T, η_M, and η_C depend on the stress tensors σ^{h} and σ^{a}, which are unique up to divergence free tensor fields. Therefore, we need to minimize $\eta(u_h) = \eta_T(u_h) + \eta_M(u_h) + \eta_C(u_h)$ with respect to the divergence free tensor field. Recall the sharp estimate for the residue (3.15), we have

$$\langle \delta\mathscr{E}^{\mathrm{a}}(I_{\mathrm{a}}u_h), v\rangle \leqslant \min_{c_a\in N_1(\mathcal{T}_a)^2, c_h\in N_1(\mathcal{T}_h)^2} \tilde{\eta}(\sigma^{\mathrm{a}}(I_{\mathrm{a}}u_h)+\nabla c_a \mathsf{J}, \sigma^{\mathrm{h}}(u_h)+\nabla c_h \mathsf{J})\|\nabla v\|_{L^2}. \quad (4.1)$$

In (4.1), we need to solve a nonlinear minimization problem with respect to c_a and c_h which are both defined over whole Ω, the dimension of c_a is $2|\mathcal{F}_h|$, and the dimension of c_h is $2|\mathcal{F}_{\mathrm{a}}|$. The cost for the exact "stress tensor correction" is proportional to solving the original energy minimisation problem if not bigger.

Here, we introduce an approximate version of "stress tensor correction", which is motivated by the explicit calculation in [36, Lemma 5.2] as well as the analysis of a/c stress tensor in [27, § 6.2.3]: a "good" a/c stress tensor can be chosen such that it equals to the atomistic stress tensor in the atomistic domain, and equals to the continuum stress tensor for uniform deformation. To be precise, we only need to apply the stress tensor correction to the modelling error η_M. In addition, we choose $c_a \equiv 0$, and $c_h(q_f) = 0$, where q_f is the midpoint of $f \in \mathcal{F}_h$, $f \bigcap \Lambda_{\mathrm{i}} = \varnothing$. Thus the only degrees of freedom to be determined are those $c_h(q_f)$ such that $f \bigcap \Lambda_{\mathrm{i}} \neq \varnothing$.

We propose the following approximate "stress tensor correction":

- Take $\sigma_0^{\mathrm{a}}(I_{\mathrm{a}}u_h)$ and $\sigma_0^{\mathrm{h}}(u_h)$ as the forms in (2.20) and (2.22) separately.
- Let $\sigma^{\mathrm{a}}(I_{\mathrm{a}}u_h) = \sigma_0^{\mathrm{a}}(I_{\mathrm{a}}u_h)$.
- Determine c_h, such that $c_h(q_f) = 0$, where q_f is the midpoint of $f \in \mathcal{F}_h$, $f \bigcap \Lambda_{\mathrm{i}} = \varnothing$, and c_h minimizes the following sum

$$\sum_{T\in\mathcal{T}_{\mathrm{a}}^{\mathrm{i}}} |T| \left[\sigma^{\mathrm{a}}(I_{\mathrm{a}}u_h, T) - \left(\sigma^{\mathrm{h}}(I_{\mathrm{a}}u_h, T) + \nabla c^h \mathsf{J}\right)\right]^2 \quad (4.2)$$

- Let $\sigma^{\mathrm{h}}(u_h) = \sigma_0^{\mathrm{h}}(u_h) + \nabla c^h \mathsf{J}$.
- Compute η_M, η_T and η_C with $\sigma^{\mathrm{a}}(I_{\mathrm{a}}u_h)$ and $\sigma^{\mathrm{h}}(u_h)$.

Instead of minimizing the overall error η with respect to c_a and c_h, we now only minimize the modeling error η_M with respect to the degrees of freedom of σ^{h} adjacent to the interface. This dramatically reduced the computational cost of "stress tensor correction", but we will see in the following numerical results that this remains sufficient to achieve optimal accuracy.

We demonstrate the effect of stress tensor correction in Figure 2. Figure 2(a) shows H^1 errors with respect to degrees of freedom N. If the stress tensor correction is applied, the error follows the optimal N^{-1} asymptotics before the saturation is reached; if the stress tensor correction is not applied, the error is suboptimal. Figure 2(b) shows the error estimator η with respect to degrees of freedom N. The N^{-1} convergence of η is much more significant with correction, and η may not even

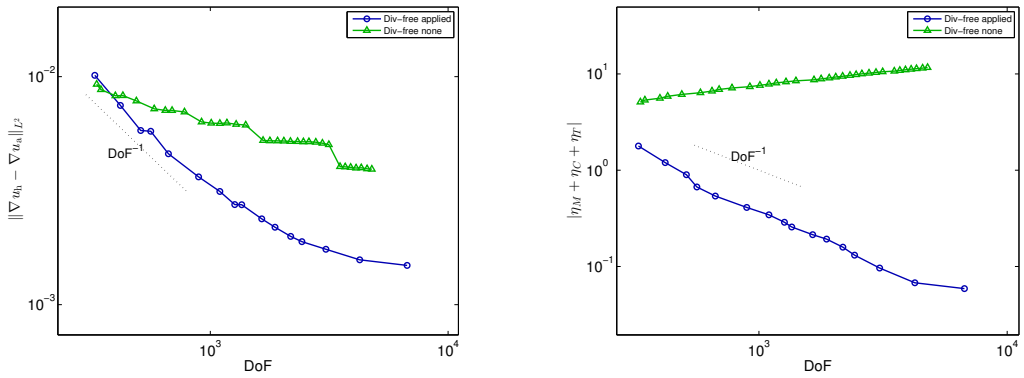

(a) H_1 error. (b) Estimator

FIGURE 2. Effect of stress tensor correction. Divacancy example, $R_c = 1000$, $\tau_1 = 0.7$, $\tau_2 = 0.2$. Figure 2(a): H_1 error vs. DoF; Figure 2(b): error estimator vs. DoF.

decrease with respect to N without correction. This is because η_M is proportional to the area of interface region without stress tensor correction, and when N increases, the area of interface region increases correspondingly.

4.1.2. *Local error estimator.* We need to assign global estimators to local elements properly, then mark and subdivide those elements which contribute most to the estimator.

Recall that from (3.8) and the stress tensor correction,

$$(\eta_M(u_h))^2 := (C^{\mathrm{Tr}})^2 \sum_{T\in\mathcal{T}_{\mathrm{a}}} |T|\big[\sigma^{\mathrm{a}}(I_{\mathrm{a}}u_h, T) - \sum_{T'\in\mathcal{T}_{\mathrm{h}}, T'\bigcap T\neq\varnothing} \frac{|T'\bigcap T|}{|T|}(\sigma_0^{\mathrm{h}}(u_h, T') + \nabla c_h \mathsf{J})\big]^2.$$

is computed in each $T \in \mathcal{T}_{\mathrm{a}}$ and summed up. We could see the contribution is 0 for those $T \in \mathcal{T}_{\mathrm{a}}$ located completely inside an element $T' \in \mathcal{T}_{\mathrm{h}}$. As a result, we need only take care of those $T \in \mathcal{T}_{\mathrm{a}}$, and $T' \in \mathcal{T}_{\mathrm{h}}$ with $T\bigcap\partial T' \neq \varnothing$. We first calculate

$$\eta_M(T, T') := |T'\bigcap T|\left[\sigma^{\mathrm{a}}(I_{\mathrm{a}}u_h, T) - \frac{|T'\bigcap T|}{|T|}(\sigma^{\mathrm{h}}(u_h, T') + \nabla c_h \mathsf{J})\right]^2.$$

for $T \in \mathcal{T}_{\mathrm{a}}$, then let $\eta_M(T') = \sum_{T\in\mathcal{T}_{\mathrm{a}}, T\bigcap T'\neq\varnothing} \eta_M(T, T')$ for element $T' \in \mathcal{T}_{\mathrm{h}}$.

Analogously, we can define the local contribution of the truncation error $\eta_T(T')$ for $T' \in \mathcal{T}_{\mathrm{h}}$, such that $\sum_{T'\in\mathcal{T}_{\mathrm{h}}} \eta_T(T') = \eta_T^2$.

Recall from (3.12) that,

$$\eta_C(u_h) := \sqrt{3}C^{\mathrm{Tr}}C'_{\mathcal{T}_{\mathrm{h}}}\Big(\sum_{f\in\mathcal{F}_h}(h_f[\![\sigma]\!])^2\Big)^{\frac{1}{2}}$$

For $T_1', T_2' \in \mathcal{T}_{\mathrm{h}}$ such that $T_1'\bigcap T_2' = f$, $f \in \mathcal{F}_h$, we define $\eta_C(T')$ as follows,

$$\eta_C(T') = \sqrt{3}C^{\mathrm{Tr}}C'_{\mathcal{T}_{\mathrm{h}}} \sum_{f\in\mathcal{F}_h\bigcap T'\in\mathcal{T}_{\mathrm{h}}} \frac{1}{2}(h_f[\![\sigma]\!]_f)^2.$$

For the energy estimator μ_E from section § 3.3.2, we can also define the local contributions correspondingly as $\mu_E(T')$ such that $\sum_{T'\in\mathcal{T}_{\mathrm{h}}} \mu_E^2(T') = \mu_E^2$.

Once we assigned the local estimators, we are ready to define the indicator ρ_T. We should emphasize that, to keep it consistent, we require that the sum of local estimators should equal to the value of global estimator.

Let

$$\rho_T = (C^{\mathrm{Tr}})^2 \frac{\eta_M(T)}{\eta_M} + (\sqrt{3} C^{\mathrm{Tr}} C'_{\mathcal{T}_{\mathrm{h}}})^2 \frac{\eta_C(T)}{\eta_C}$$

Meanwhile, for the energy based estimate, we have,

$$\rho_T^E = C^E (C^{\mathrm{Tr}})^2 \left(\eta_M(T)\right)^2 + C^E (\sqrt{3} C^{\mathrm{Tr}} C'_{\mathcal{T}_{\mathrm{h}}})^2 \left(\eta_C(T)\right)^2 + |\mu_E(T)| \tag{4.3}$$

Algorithm 4.1. *A posteriori mesh refinement.*

Step 0 Prescible $N_{\max}$, ρ_{tol}, τ_1, τ_2.

Step 1 Solve: Solve the a/c solution of (2.11) *on the current mesh* $\mathcal{T}_{\mathrm{h}}$. *Compute the error indicator* ρ_T *for* $T \in \mathcal{T}_{\mathrm{h}}$. *Set* $\rho_T = 0$ *for* $T \in \mathcal{T}_{\mathrm{a}} \bigcap \mathcal{T}_{\mathrm{h}}$.

Step 2.1 Mark 1: Choose a minimal subset $\mathcal{M} \subset \mathcal{T}_{\mathrm{h}}$ *such that*

$$\sum_{T \in \mathcal{M}} \rho_T \leqslant \frac{1}{2} \sum_{T \in \mathcal{T}_{\mathrm{h}}} \rho_T.$$

Step 2.2 Mark 2: Find the interface elements $\mathcal{M}_{\mathrm{i}} := \{T \in \mathcal{M} : T \bigcap \Lambda_{\mathrm{i}} \neq \varnothing\}$. *Check if*

$$\sum_{T \in \mathcal{M}_{\mathrm{i}}} \rho_T \geqslant \tau_1 \sum_{T \in \mathcal{M}} \rho_T. \tag{4.4}$$

where tolerance $0 < \tau_1 < 1$. *If true, let* $\mathcal{M} = \mathcal{M} \backslash \mathcal{M}_{\mathrm{i}}$.

Step 3 Refine: If (4.4) *is true, expand interface* Λ_{i} *outward by one layer. Then, bisect all elements* $T \in \mathcal{M}$.

Step 4 Estimate: Compute the degrees of freedom N, *error estimator* ρ_T *and* $\rho = \sum_T \rho_T$. *If the* $N > N_{\max}$ *or* $\rho < \rho_{\mathrm{tol}}$, *stop; otherwise, go to Step 1.*

Remark 4.1. There are many possibilities to modify the above algorithms, for example,

Step 2.1: Choose a minimal subset $\mathcal{M}$, s.t.

$$\rho_T \geqslant \mathrm{mean}(\rho), \quad \forall T \in \mathcal{M}.$$

Step 2.2: *Mark 2:* We can find the interface elements which are within k layers of atomistic distance, $\mathcal{M}_{\mathrm{i}}^k := \{T \in \mathcal{M} \bigcap \mathcal{T}_{\mathrm{h}}^{\mathrm{c}} : \mathrm{dist(T, \Lambda^i)} \leqslant \mathrm{k}\}$. Check what is the first $k \leqslant K$ such that

$$\sum_{T \in \mathcal{M}_{\mathrm{i}}^k} \rho_T \geqslant \tau_1 \sum_{T \in \mathcal{M}} \rho_T, \tag{4.5}$$

where tolerance $0 < \tau_1 < 1$. If true, let $\mathcal{M} = \mathcal{M} \backslash \mathcal{M}_{\mathrm{i}}^k$. Then in step 3, expand interface Λ_{i} outward by k layers.

Step 4: Compute the convergence rate β of the estimator of the adaptive algorithm ρ with respect to the degrees of freedom N. If $\beta \leqslant \tau_2$, stop, otherwise goto step 1. □

Remark 4.2. After pushing the interface outward in Step 3, we have to 'remove' those triangles in the continuum mesh which overlap with the new atomistic triangulation. It will produce a gap between atomistic and continuum regions. We need to triangulate this gap, and adjust the positions of the nodes to improve the

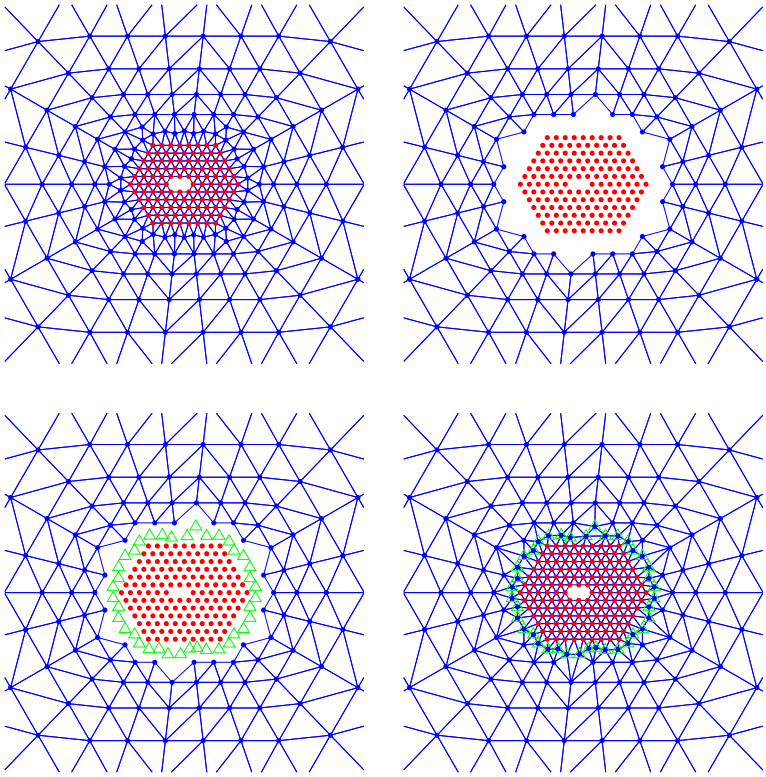

FIGURE 3. Captures of invoking *EasyMesh*. (Top-left) initial mesh with $R_a = 5$; (Top-right) mesh with $R_a = 6$ before calling *EasyMesh*; (Bottom-left) generating nodes, marked with green triangles; (Bottom-right) forming triangulations.

quality of the interfacial triangles. In our implementation, we use the *EasyMesh*, a two-dimentional quality mesh generator to carry out this task [24]. □

4.2. **Model Problem.** Recall the EAM potential defined in (2.5). Let

$$\phi(r) = \exp(-2a(r-1)) - 2\exp(-a(r-1)), \quad \psi(r) = \exp(-br)$$

$$F(\tilde{\rho}) = C\left[(\tilde{\rho} - \tilde{\rho}_0)^2 + (\tilde{\rho} - \tilde{\rho}_0)^4\right]$$

with the parameter $a = 4, b = 3, c = 10$ and $\tilde{\rho}_0 = 6\exp(0.9b)$, which is consistent with the numerical experiments in the a priori analysis [37].

To generate a defect, we remove k atoms from Λ^{hom},

$$\begin{aligned} \Lambda_k^{\text{def}} &:= \{-(k/2)e_1, \dots, (k/2-1)e_1)\}, \qquad \text{if} \quad k \quad \text{is even}, \\ \Lambda_k^{\text{def}} &:= \{-(k-1)/2e_1, \dots, (k-1)/2e_1)\}, \qquad \text{if} \quad k \quad \text{is odd}, \end{aligned}$$

and $\Lambda = \Lambda^{\text{hom}} \backslash \Lambda_k^{\text{def}}$. See Figure 4 for an illustration.

For $\ell \in \Lambda$, consider the nearest neighbour interaction, $\mathcal{N}_\ell := \{\ell' \in \Lambda \,|\, 0 < |\ell' - \ell| \leqslant 1\}$, and interaction range $\mathcal{R}_\ell := \{\ell' - \ell \,|\, \ell' \in \mathcal{N}_\ell\} \subseteq \{a_j, j = 1, \dots, 6\}$. The defect core D^{def} can be defined by $D^{\text{def}} = \{\ell \in \Lambda : \exists 1 \leqslant j \leqslant 6, \ell + a_j \in \Lambda_k^{\text{def}}\}$, which is the first layer of atoms around Λ_k^{def}.

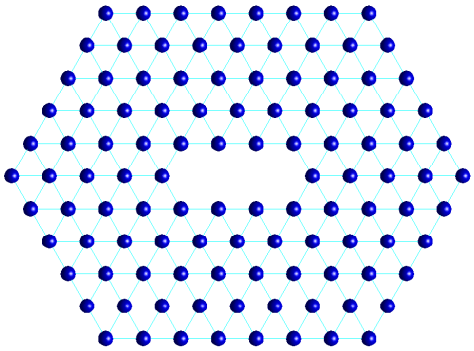

FIGURE 4. Illustration of the atomistic lattice Λ with 3 vacancies surrounded by 5 atomistic layers.

4.3. **Di-vacancy Example.** In this section, we numerically justify the performance of the proposed adaptive mesh refinement algorithm. We take the same di-vacancy example in [37], namely, setting $k = 2$ for Λ_k^{def}. We apply isotropic stretch S and shear γ_{II} by setting

$$\mathsf{B} = \begin{pmatrix} 1+\mathrm{S} & \gamma_{II} \\ 0 & 1+\mathrm{S} \end{pmatrix} \cdot \mathsf{F}_0$$

where $\mathsf{F}_0 \propto \mathrm{I}$ minimizing W, $\mathrm{S} = \gamma_{II} = 0.03$

4.3.1. *Fix computation domain.* In this subsection, we fix $R_c = 1000$. The numerical results are shown in Figure 5 and Figure 6. The red dashed lines in both figures denote the truncation errors η_T and η_T^2 respectively. The figures show that when N is small, the modelling error and coarsening error dominates, our results coincide with the optimal a priori convergence rate (N^{-1} for H^1 norm and N^{-2} for energy, respectively). When N increases, the truncation error becomes dominant, which results in a suboptimal convergence rate and finally saturates the overall error. These results indicate that for a fixed computational domain, we can only achieve optimal convergence rate up to a certain critical degree of freedom. A possible cure is to enlarge the computational domain in order to balance the truncation error with the modeling and coarsening errors, which motivates the next numerical experiments.

4.3.2. *Error with respect to domain size: the effect of the truncation error.* We consider computational domains of different sizes in this section. Let $R_a = [6, 15, 30]$, and $R_c = (R_a + 1)^2 + 10$ which follows from a priori analysis. We terminate the adaptive algorithm when the degree of freedom exceeds $30R_a^2$.

The numerical results in Figure 7 and Figure 8 suggest that by considering the truncation error of the finite size computational domain, we may change the computational domain automatically in the adaptive algorithm in order to maintain the optimal convergence rate with respect to the degrees of freedom. This will be done in a future work.

5. CONCLUSION

We derive rigorous a posteriori error estimates for a class of consistent (ghost force free) atomistic/continuum coupling schemes. Numerical results for the corresponding adaptive mesh refinement algorithms based on the error estimator are optimal

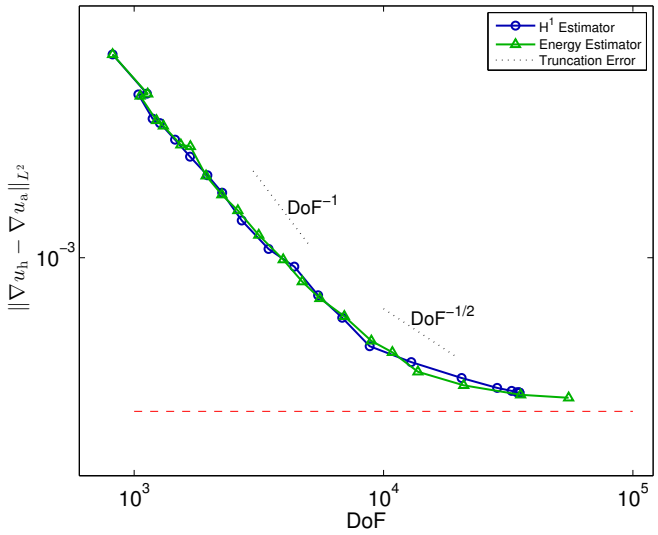

FIGURE 5. H^1 error vs. N, $R_c = 1000$, $\tau_1 = 0.7$, $\tau_2 = 0.2$.

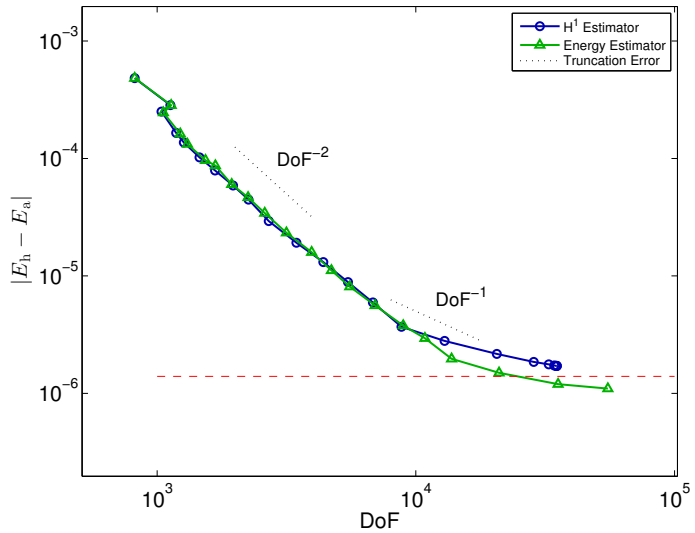

FIGURE 6. Energy error vs. N, $R_c = 1000$, $\tau_1 = 0.7$, $\tau_2 = 0.2$.

compare to a priori analysis. This opens an avenue for further mathematical analysis and algorithmic developments for longer range interactions, higher dimensional problems, and general atomistic/continuum coupling algorithms.

6. Appendix

6.1. **Extension to the vacancies.** We need to extend v from Λ to $\Lambda^{\rm hom}$ which includes the vacancy sites. We first define the extension operator E on $\mathscr{U}$ by

$$Eu := \operatorname*{argmin}_{v\in\mathscr{U}, v=u \text{ on } \Lambda} \Phi_{\mathbb{B}}(v) := \operatorname{argmin} \sum_{b\in\mathbb{B}} |\rho_b \cdot D_b v|^2, \quad \forall u \in \mathscr{U}, \tag{6.1}$$

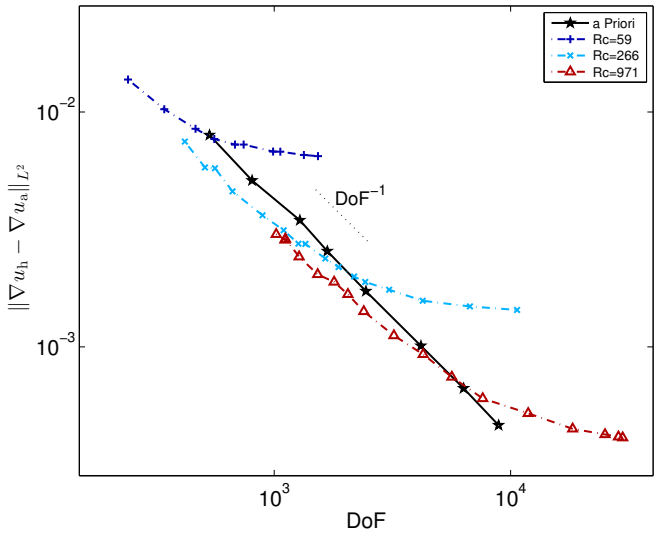

FIGURE 7. H^1 error vs. N, for $R_c = 59, 266, 971$, respectively.

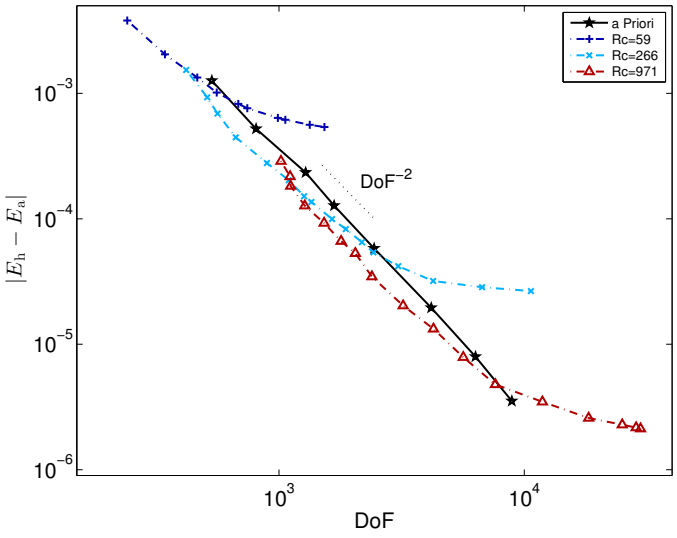

FIGURE 8. Energy error vs. N, for $R_c = 59, 266, 971$, respectively.

where $\mathbb{B}$ defined in (3.17) is the set of all nearest-neighbour interaction bonds in Λ^{hom}. Notice that for $v \in \mathscr{U}$, $\|\nabla v\|_{L^2}$ can be properly and uniquely defined by $\|\nabla Ev\|_{L^2}$.

It is known from [31, Proposition 4.1] that $\Phi_{\mathbb{B}}(v)$ is equivalent to $\|\nabla v\|_{L^2}$ such that,

$$\frac{3}{4}\|\nabla v\|_{L^2}^2 \leqslant \Phi_{\mathbb{B}}(v) \leqslant \frac{9}{4}\|\nabla v\|_{L^2}^2 \tag{6.2}$$

Since $\mathsf{A}^{-1}E\mathsf{A}v = Ev$ on Λ, by definition of Ev, we have $\Phi_{\mathbb{B}}(\mathsf{A}^{-1}E\mathsf{A}v) \geqslant \Phi_{\mathbb{B}}(Ev)$. Combined with the inequality $\|\mathsf{GH}\|_F \leqslant \|\mathsf{G}\|_F\|\mathsf{H}\|_F$ for the matrix Frobenius norm

and (6.2), it holds that,

$$\begin{aligned}\|\nabla Ev\|_{L^2}^2 &\leqslant \frac{4}{3}\Phi_{\mathbb{B}}(Ev)\\ &\leqslant \frac{4}{3}\Phi_{\mathbb{B}}(\mathsf{A}^{-1}E\mathsf{A}v)\\ &\leqslant 3\|\nabla \mathsf{A}^{-1}E\mathsf{A}v\|_{L^2}^2\\ &\leqslant 3\|\mathsf{A}^{-1}\|_F\|\nabla E\mathsf{A}v\|_{L^2}^2. \end{aligned} \tag{6.3}$$

References

[1] M. Arndt and M. Luskin. Error estimation and atomistic-continuum adaptivity for the quasicontinuum approximation of a Frenkel-Kontorova model. SIAM J. Multiscale Modeling & Simulation, 7:147–170, 2008.

[2] M. Arndt and M. Luskin. Goal-oriented adaptive mesh refinement for the quasicontinuum approximation of a Frenkel-Kontorova model. Computer Methods in Applied Mechanics and Engineering, 197:4298–4306, 2008.

[3] C. Carstensen and R. Verfürth. Edge residuals dominate a posteriori error estimates for low order finite element methods,. SIAM J. Numer. Anal., 36(5):1571–1587, 1999.

[4] Ph. Clément. Approximation by finite element functions using local regularization. ESAIM: Mathematical Modelling and Numerical Analysis - Modélisation Mathématique et Analyse Numérique, 9(R2):77–84, 1975.

[5] M. S. Daw and M. I. Baskes. Embedded-Atom Method: Derivation and Application to Impurities, Surfaces, and other Defects in Metals. Physical Review B, 20, 1984.

[6] M. Dobson and M. Luskin. An analysis of the effect of ghost force oscillation on quasicontinuum error. M2AN Math. Model. Numer. Anal., 43(3):591–604, 2009.

[7] W. E, J. Lu, and J. Z. Yang. Uniform accuracy of the quasicontinuum method. Phys. Rev. B, 74(21):214115, 2006.

[8] W. E and P. Ming. Cauchy-Born rule and the stability of crystalline solids: static problems. Arch. Ration. Mech. Anal., 183(2):241–297, 2007.

[9] V. Ehrlacher, C. Ortner, and A. V. Shapeev. Analysis of boundary conditions for crystal defect atomistic simulations. Arch. Rat. Mech. Anal., 222(3):1217–1268, 2016.

[10] L. D. Fang, C. Ortner, and L. Zhang. Atomistic/continuum coupling in 3d. manuscript.

[11] M. W. Finnis and J. E. Sinclair. A simple empirical n-body potential for transition-metals. Philos. Mag. A, 50(1):45–55, 1984.

[12] H. Fischmeister, H. Exner, M.-H. Poech, S. Kohlhoff, P. Gumbsch, S. Schmauder, L. S. Sigi, and R. Spiegler. Modelling fracture processes in metals and composite materials. Z. Metallkde., 80:839–846, 1989.

[13] Michael Grant and Stephen Boyd. CVX: Matlab software for disciplined convex programming, version 2.1. `http://cvxr.com/cvx`, March 2014.

[14] X. H. Li, C. Ortner, A. V. Shapeev, and B. Van Koten. Analysis of blended atomistic/continuum hybrid methods. Numerische Mathematik, 134(2):275–326, 2016.

[15] P. Lin. Convergence analysis of a quasi-continuum approximation for a two-dimensional material without defects. SIAM J. Numer. Anal., 45(1):313–332 (electronic), 2007.

[16] P. Lin and A. V. Shapeev. Energy-based ghost force removing techniques for the quasicontinuum method. arXiv:0909.5437.

[17] J. Lu and P. Ming. Convergence of a force-based hybrid method for atomistic and continuum models in three dimension. Comm. Pure Appl. Math., 66:83–108, 2013.

[18] M. Luskin and C. Ortner. An analysis of node-based cluster summation rules in the quasicontinuum method. SIAM Journal on Numerical Analysis, 47(4):3070–3086, 2009.

[19] M. Luskin and C. Ortner. Atomistic-to-continuum-coupling. Acta Numerica, 2013.

[20] M. Luskin, C. Ortner, and B. Van Koten. Formulation and optimization of the energy-based blended quasicontinuum method. Comput. Methods Appl. Mech. Engrg., 253, 2013.

[21] C. Makridakis, D. Mitsoudis, and P. Rosakis. On atomistic-to-continuum couplings without ghost forces in three dimensions. Appl. Math. Res. Express, 2014(1):87–113, 2014.

[22] R. Miller and E. Tadmor. A unified framework and performance benchmark of fourteen multiscale atomistic/continuum coupling methods. Modelling Simul. Mater. Sci. Eng., 17, 2009.
[23] P. Ming and J. Z. Yang. Analysis of a one-dimensional nonlocal quasi-continuum method. Multiscale Modeling & Simulation, 7(4):1838–1875, 2009.
[24] B. Niceno. EasyMesh: A two-dimensional quality mesh generator. `http://web.mit.edu/easymesh_v1.4/www/easymesh.html`.
[25] M. Ortiz, R. Phillips, and E. B. Tadmor. Quasicontinuum analysis of defects in solids. Philosophical Magazine A, 73(6):1529–1563, 1996.
[26] C. Ortner. A priori and a posteriori analysis of the quasi-nonlocal quasicontinuum method in 1D. Math. Comp., 80(275):1265–1285, 2011.
[27] C. Ortner. The role of the patch test in 2D atomistic-to-continuum coupling methods. ESAIM Math. Model. Numer. Anal., 46, 2012.
[28] C. Ortner, A. Shapeev, and L. Zhang. (in-)stability and stabilisation of qnl-type atomistic-to-continuum coupling methods. ArXiv e-prints, 1308.3894, 2013.
[29] C. Ortner and A. V. Shapeev. Analysis of an energy-based atomistic/continuum coupling approximation of a vacancy in the 2d triangular lattice. ArXiv e-prints, 2011.
[30] C. Ortner and A. V. Shapeev. Interpolation of lattice functions and applications to atomistic/continuum multiscale methods. ArXiv e-prints, arXiv:1204.3705, 2012.
[31] C. Ortner and A. V. Shapeev. Analysis of an energy-based atomistic/continuum coupling approximation of a vacancy in the 2d triangular lattice. Math. Comp., 82:2191–2236, 2013.
[32] C. Ortner and E. Süli. Analysis of a quasicontinuum method in one dimension. M2AN Math. Model. Numer. Anal., 42(1):57–91, 2008.
[33] C. Ortner and F. Theil. Justification of the cauchy–born approximation of elastodynamics. Arch. Ration. Mech. Anal., 207, 2013.
[34] C. Ortner and H. Wang. A priori error estimates for energy-based quasicontinuum approximations of a periodic chain. Math. Models Methods Appl. Sc., 21:2491–2521, 2011.
[35] C. Ortner and H. Wang. A posteriori error control for a quasi-continuum approximation of a periodic chain. IMA Journal of Numerical Analysis, 34(3):977–1001, 2013.
[36] C. Ortner and L. Zhang. Construction and sharp consistency estimates for atomistic/continuum coupling methods with general interfaces: a 2D model problem. SIAM J. Numer. Anal., 50, 2012.
[37] C. Ortner and L. Zhang. Energy-based atomisitic-to-continuum coupling without ghost forces. Comput. Methods Appl. Mech. Engrg., 279(1):29–45, 2014.
[38] C. Ortner and L. Zhang. Atomistic/continuum blending with ghost force correction. SIAM J. Sci. Comput., 38(1):A346–A375, 2016.
[39] S. Prudhomme, P. T. Bauman, and J. T. Oden. Error control for molecular statics problems. International Journal for Multiscale Computational Engineering, 4(5-6):647–662, 2006.
[40] A. V. Shapeev. Consistent energy-based atomistic/continuum coupling for two-body potentials in one and two dimensions. Multiscale Modeling & Simulation, 9(3):905–932, 2011.
[41] A. V. Shapeev. Consistent energy-based atomistic/continuum coupling for two-body potentials in three dimensions. SIAM J. Sci. Comput., 34(3):B335–B360, 2012.
[42] V. B. Shenoy, R. Miller, E. B. Tadmor, D. Rodney, R. Phillips, and M. Ortiz. An adaptive finite element approach to atomic-scale mechanics–the quasicontinuum method. J. Mech. Phys. Solids, 47(3):611–642, 1999.
[43] T. Shimokawa, J. J. Mortensen, J. Schiotz, and K. W. Jacobsen. Matching conditions in the quasicontinuum method: Removal of the error introduced at the interface between the coarse-grained and fully atomistic region. Phys. Rev. B, 69(21):214104, 2004.
[44] E. B. Tadmor and R. E. Miller. Modeling Materials: Continuum, Atomistic and Multiscale Techniques. Cambridge University Press, 2012.
[45] I. Tembhekar, J. S. Amelang, L. Munk, and D. M. Kochmann. Automatic adaptivity in the fully-nonlocal quasicontinuum method for coarse-grained atomistic simulations. Int. J. Numer. Meth. Engng., 2016.
[46] R. Verfürth. A Review of A Posteriori Error Estimation and Adaptive Mesh-Refinement Techniques. John Wiley & Sons Ltd., 1996.
[47] R. Verfürth. Error estimates for some quasi-interpolation operators. M2AN Math. Model. Numer. Anal., 33(4):695–713, 1999.

Hao Wang, College of Mathematics, Sichuan University, No. 24 South Section One, Yihuan Road, Chengdu, 610065, China
E-mail address: wangh@scu.edu.cn

Mingjie Liao, Department of Applied Mathematics and Mechanics, University of Science and Technology Beijing, No. 30 Xueyuan Road, Haidian District, Beijing 100083, China
E-mail address: mliao@xs.ustb.edu.cn

Ping Lin, Department of Mathematics, University of Dundee, Dundee, DD1 4HN, Scotland, United Kingdom
E-mail address: plin@maths.dundee.ac.uk

Lei Zhang, Department of Mathematics, Institute of Natural Sciences, and Ministry of Education Key Laboratory of Scientific and Engineering Computing (MOE-LSC), Shanghai Jiao Tong University, 800 Dongchuan Road, Shanghai 200240, China
E-mail address: lzhang2012@sjtu.edu.cn